A Switched Systems Approach to Multiagent System Consensus: A Relay–Explorer Perspective

Federico M. Zegers, *Member, IEEE*, Patryk Deptula, Hsi-Yuan Chen, Axton Isaly, and Warren E. Dixon, *Fellow, IEEE*

***Abstract*— The rendezvous or position consensus problem is a fundamental topic within the multiagent system (MAS) literature and has numerous engineering applications. The majority of recent results that solve the position consensus problem rely on communication networks and each agent's ability to obtain position information via direct measurements and communication. Distributed coordination strategies for MASs that are network free and have agents that cannot directly measure position information are scarce. In this work, we develop a relay–explorer strategy to achieve position consensus at a common, desired location. In particular, a group of explorer agents, lacking global position sensors, use open-loop estimators of their position to independently dead reckon toward the desired location. To prevent the difference between the estimated and true position of each explorer from growing beyond a user-defined threshold, a mobile information service provider (relay agent) that is capable of measuring its position in the global coordinate frame, intermittently visits each explorer to provide position information as determined by a maximum dwell-time condition. The relay agent has a position estimator for each explorer, and each estimator is synchronized with the corresponding explorer. The relay agent uses these position estimators to locate each explorer, maneuver to them, and provide position feedback. The contribution of this work over our precursory results is the consideration of uncertain explorer agent dynamics, which are estimated online using recurrent neural networks and integral concurrent learning. The estimated dynamics serve as feed-forward model approximations in the position estimators used by the explorers and relay agent, which generate more accurate position estimates once a finite excitation condition is satisfied. The MAS is modeled as a switched system, and a Lyapunov-based analysis is used to derive a maximum dwell-time condition for each explorer, prove the MAS is exponentially regulated to the desired location, and show the error between the estimated and true explorer dynamics is uniformly ultimately bounded. Experiments and multiple simulation examples are provided to verify the theoretical development, explore the scalability and learning performance of the approach, and shed light on future extensions.**

***Index Terms*—Adaptive control, consensus algorithm, Lyapunov methods, multiagent systems, network control.**

Manuscript received 16 February 2022; revised 15 July 2022; accepted 4 August 2022. Date of publication 13 January 2023; date of current version 8 February 2023. This work was supported in part by the Office of Naval Research under Grant N00014-13-1-0151 and in part by AFOSR under Grant FA9550-18-1-0109 and Grant FA9550-19-1-0169. This paper was recommended for publication by Associate Editor N. Gans and Editor P. Robuffo Giordano upon evaluation of the reviewers comments. *(Corresponding author: Federico M. Zegers.)*

Federico M. Zegers, Axton Isaly, and Warren E. Dixon are with the Department of Mechanical and Aerospace Engineering, University of Florida, Gainesville, FL 32611 USA (e-mail: fredzeg@ufl.edu; axtonisaly1013@ufl.edu; wdixon@ufl.edu).

Patryk Deptula is with the Charles Stark Draper Laboratory, Inc., Cambridge, MA 02139-3539 USA (e-mail: pdeptula@ufl.edu).

Hsi-Yuan Chen is with the Amazon Robotics, North Reading, MA 01864-2622 USA (e-mail: hychen@ufl.edu).

Color versions of one or more figures in this article are available at https://doi.org/10.1109/TRO.2022.3200005.

Digital Object Identifier 10.1109/TRO.2022.3200005

I. Introduction

DISTRIBUTED control of network systems has been an active area of research for the past two decades. Distributed algorithms have been developed for state estimation [1], impedance-based cooperative manipulation [2], formation control [3], and multiagent coverage [4]. A fundamental topic within the network control literature is consensus, especially rendezvous or position consensus, which is when the positions of all agents in a multiagent system (MAS) are brought into agreement. The results in [5], [6], and [7], which can be used to achieve rendezvous, employ distributed consensus algorithms and the exchange of state information between neighboring agents over a communication network.

To reduce the amount of communication within a network, researchers investigated event/self-triggered control, where sampled data are provided to network agents only when desired stability and/or performance specifications trigger the need [8], [9], [10], [11], [12], [13], [14], [15]. In [8], self-triggering enables the reduction of communication when the system is close to equilibrium. In [9], event-triggered mechanisms enable intermittent communication in the sensor-to-control channels and control-to-actuator channels, leading to model-based periodic event-triggered control for discrete-time linear plants. In [10], intermittent communication is extended to MASs by using a sampled-data event detector, which improves on continuous event detectors and leads to a reduction in the communication requirement between neighboring agents. An event-triggered communication approach facilitating leader–follower consensus for second-order systems subject to fixed and switching network topologies is provided in [12]. The result in [13] improves upon [12] by solving the leader–follower consensus problem for linear time-invariant (LTI) systems while using event-triggered communication over fixed and switching network topologies. Similarly, the results in [14] and [15] extend the event-triggered development in [13] to scenarios where cooperative agents are subjected to malicious state information originating from corrupted neighbors. While event/self-triggered control can alleviate the communication burden, MAS coordination over a mobile network may constrain the spatial geometry of the MAS to maintain the connectivity of the communication graph. Such geometric constraints motivate the development of a spatially relaxed coordination scheme that accommodates intermittent communication.

Another approach for MAS coordination is to use indirect communication between agents through a central base station. The results in [16], [17], and [18] consider the case where communication between agents and the outside world cannot occur at any desired time. Indirect communication between agents is only possible at specific instants, such as in [19], e.g., when a submarine surfaces to communicate with a cloud. The results in [16] and [17] achieve position consensus and formation assembly, respectively, by using self-triggered communication. In [18], team-triggered communication is utilized to attain asymptotic consensus while preventing Zeno behavior.

A common characteristic of all the aforementioned results is that each agent can independently measure either their position in the global coordinate frame or the relative position between themselves and their neighbors. Consequently, MASs with agents that cannot locate themselves cannot use any of the previously mentioned strategies to coordinate. Moreover, the works in [10], [12], [13], [14], and [15] assume the communication graph is either always connected or jointly connected, which is a strong assumption since graph connectivity is a distance-dependent property in mobile networks. Once the communication graph becomes disconnected (jointly disconnected), these algorithms fail to achieve their control objective.

Building on our previous results in [20] and [21], this article considers a unique relay–explorer consensus problem consisting of a single relay agent and multiple explorers. The relay agent has sufficient sensing capabilities to measure its position within the global coordinate frame, whereas each explorer lacks absolute position sensors. The objective of this work is to develop a control strategy that enables the explorers to rendezvous at a desired location through the use of open-loop control, whereas the relay agent ferries position information to each explorer sufficiently often to render the explorers' use of open-loop navigation viable. This work is similar to event/self-triggered methods because position feedback for the explorers is intermittent and a dwell-time trigger indicates when feedback is required. Unlike typical consensus problems, the development in this article does not consider explorer-to-explorer communication. The relay agent behaves as a mobile information service provider, and therefore, an elaborate graph structure coupling the explorers is not required. Moreover, we do not use a star graph to model the communication between the relay agent and explorers. The relay agent has a fixed communication radius and cannot provide position feedback to any explorer outside the communication radius. Service discretion is also produced through intermittent and local relay–explorer communication, allowing for flexibility in coordination. Because our result does not employ a communication graph, graph connectivity is irrelevant, and the explorers have more freedom to move as desired. Moreover, our strategy can achieve position consensus even though not every agent can measure their position within the global coordinate frame, unlike the results in [10], [11], [12], [13], [14], and [15].

Different from [20], this work assumes the dynamics of each explorer are unknown. While [21] enhances [20] by employing a two-layer neural network (NN) to generate a position estimate for each explorer, the NN weights of the estimator are continuously updated using position estimates, even when position information of the explorer is not available. Such a strategy may lead to degraded position estimation, especially when the estimated position of an explorer drifts from its true position. Therefore, we build on [20] and [21] by considering uncertain explorer dynamics that are approximated with a recurrent neural network (RNN), where the weights of each RNN are only updated when position information is available and a finite excitation condition is satisfied. While the intermittent update of RNN weights leads to less computation, the need for position feedback to facilitate weight updates requires the relay agent to linger with each explorer. The need to linger for learning leads to a more complicated switched system and a more detailed switched systems analysis. Nevertheless, the use of RNNs can lead to improved explorer model approximation and explorer locating by the relay agent.

A nonsmooth Lyapunov stability analysis shows that the switched system is exponentially regulated to a neighborhood of the desired consensus location. Exponential regulation to the consensus point is possible as a special case. In addition, using RNNs with integral concurrent learning (ICL) renders the error between the estimated and true explorer dynamics uniformly ultimately bounded (UUB). Experimental results validate the development and show that open-loop navigation by the explorers can be used to facilitate consensus provided the relay agent supplies position information according to each explorer's maximum dwell-time condition. Simulation results show the satisfaction of a finite excitation condition, which implies the uncertain explorer dynamics can be better approximated. More accurate model knowledge of the explorer dynamics leads to a slower accumulation of error and better regulation to the consensus point. Moreover, since the relay agent uses the explorer position estimates to locate each explorer, explorer locating is enhanced and the frequency of servicing can be reduced due to the slower accumulation of error. Simulations are also conducted to further verify the development, investigate the scalability of the strategy, and highlight the benefits of using RNNs with ICL.

The rest of this article is organized as follows. Section II introduces relevant notation. Sections III–V discuss the agent dynamics, objective, and the control strategy, respectively. Sections VI and VII provide a stability analysis for the switched system and experiments, respectively. Section VIII presents simulation results under various configurations. Finally, Section IX concludes this article.

II. Notation

Let $\mathbb{R}$ and $\mathbb{Z}$ denote the set of real numbers and integers, respectively, where $\mathbb{R}_{\geq 0} \triangleq [0, \infty)$,$\mathbb{R}_{>0} \triangleq (0, \infty)$, $\mathbb{Z}_{\geq 0} \triangleq \mathbb{R}_{\geq 0} \cap \mathbb{Z}$, and $\mathbb{Z}_{>0} \triangleq \mathbb{R}_{>0} \cap \mathbb{Z}$. Given $M \in \mathbb{Z}_{>0}$, let $[M] \triangleq \{1, 2, \ldots, M\}$. The maximum and minimum eigenvalues of $A = A^\top \in \mathbb{R}^{n \times n}$ are $\lambda_{\max}(A) \in \mathbb{R}$ and $\lambda_{\min}(A) \in \mathbb{R}$, respectively. The $p \times q$ zero matrix and the $p \times 1$ zero-column vector are denoted by $0_{p \times q}$ and 0_p, respectively. The $p \times p$ identity matrix is denoted by I_p. The Euclidean norm of $r \in \mathbb{R}^n$ is $\|r\| \triangleq \sqrt{r^\top r}$. Let $\otimes$ and $\mathrm{vec}(\cdot)$ denote the Kronecker product and vectorization transformation, respectively. Given $H \in \mathbb{R}^{m \times n}$

with columns $\{h_i\}_{i\in[n]} \subset \mathbb{R}^m$, $\mathrm{vec}(H) = [h_1^\top, h_2^\top, \ldots, h_n^\top]^\top \in \mathbb{R}^{mn}$. The set of bounded functions $f : \mathbb{R}^m \to \mathbb{R}^n$ is denoted by $\mathcal{L}_\infty$, where $g \in \mathcal{L}_\infty$ if and only if $\inf\{C \geq 0 : \forall_{x\in\mathbb{R}^m} \|g(x)\| \leq C\} < \infty$. The trace of $A \in \mathbb{R}^{n\times n}$ is denoted by $\mathrm{tr}(A)$. The complement of the set $\mathcal{S}$ is denoted by $\mathcal{S}^C$. For $a \triangleq [a_1, a_2, \ldots, a_m]^\top \in \mathbb{R}^m$, the signum function $\mathrm{sgn} : \mathbb{R}^m \rightrightarrows [-1, 1]^m$ is $\mathrm{sgn}(a) = [\mathrm{sgn}(a_1), \mathrm{sgn}(a_2), \ldots, \mathrm{sgn}(a_m)]^\top$, where $\mathrm{sgn}(a_i) \triangleq 1$ for $a_i > 0$, $\mathrm{sgn}(a_i) \triangleq [-1, 1]$ for $a_i = 0$, and $\mathrm{sgn}(a_i) \triangleq -1$ for $a_i < 0$.

III. System Model

Consider a MAS composed of $N \in \mathbb{Z}_{>0}$ explorer agents, indexed by $F \triangleq [N]$, and a single relay agent, indexed by 0. The motion model of agent $i \in F \cup \{0\}$ is defined as

$$\dot{p}_i = f_i(p_i) + u_i + d_i, \tag{1}$$

where $p_i \in \mathbb{R}^m$ denotes the position, $f_i : \mathbb{R}^m \to \mathbb{R}^m$ is an uncertain and locally Lipschitz function, $u_i \in \mathbb{R}^m$ denotes the control input, and $d_i : [0, \infty) \to \mathbb{R}^m$ is a bounded and locally Lipschitz function modeling an additive disturbance. For each $i \in F$ and all $t \geq 0$, $\|d_i(t)\| \leq \overline{d}_i \in \mathbb{R}_{>0}$. For simplicity, $f_0(p_0) \triangleq 0_m$ and $d_0 \equiv 0_m$, where the motion model of the relay agent becomes

$$\dot{p}_0 = u_0. \tag{2}$$

Within this work, the initial position $p_i(0)$ of explorer i is known to explorer i and the relay agent for each $i \in F$. Moreover, the relay agent can measure its own position $p_0(t)$ for all $t \geq 0$. Note that, for each $i \in F \cup \{0\}$, each position p_i is expressed within the same global coordinate frame.

Remark 1: In this work, we treat p_i as the position variable of agent $i \in F \cup \{0\}$ for simplicity. Nevertheless, p_i can also represent the pose of agent i allowing for control in both position and orientation. In such a case, the relay agent can supply pose information to each explorer and facilitate the consensus objective provided the relay agent has sufficient sensing to determine the orientation of the explorer agent in the global coordinate system. For example, the relay agent can use a camera to determine the relative orientation and then use its knowledge of its own orientation to communicate to the explorer agent its absolute orientation. Moreover, more complex relay agent dynamics, e.g., Euler–Lagrange dynamics, can also be considered. The single integrator model is used here for simplicity, and without loss of generality, to highlight the novelty of the considered problem and control strategy. The critical property the controller of the relay agent must satisfy is exponential regulation of the relay agent position to the estimated position of an explorer, which can be treated as a time-varying trajectory. Depending on the selected relay agent dynamics, standard results in literature can be leveraged to achieve trajectory regulation for certain classes of LTI, nonlinear control-affine, and Euler–Lagrange systems.

IV. Objective

The objective is to regulate the relay agent and every explorer to a desired, common, and time-invariant position $p_d \in \mathbb{R}^m$, where the objective is satisfied when $p_d - p_i$ is UUB for all $i \in F \cup \{0\}$.[1] Note that the desired position p_d is expressed within the same global coordinate frame as the $\{p_i\}_{i\in F\cup\{0\}}$. The overall challenge, which results in multiple subchallenges, is that the explorers do not have absolute position sensors but are required to converge to p_d. The first challenge is perturbations on an explorer's dynamics, which can lead to an accumulation of error between the true and estimated position. Hence, open-loop (i.e., dead reckoning) navigation methods can become increasingly inaccurate unless corrected.

To reset the accumulated error, the relay agent intermittently provides position information to each explorer. However, the relay agent may be required to travel to an explorer, which is outside its communication range, to supply the necessary position feedback. The second challenge is that the relay agent needs to predict the position of each explorer well enough to enable explorer locating and the supplying of position information; otherwise, the explorer will be lost and the resulting error system will become unstable. One technique for explorer locating is to have the relay agent use a predictor, which estimates an explorer's position through an approximation of the explorer's dynamics. The relay agent can then travel to the estimated explorer position, and if the explorer is within the communication radius of the relay agent once at the estimated position, then servicing can be performed. However, the explorer dynamics are unknown, and inaccurate models can result in an increased rate of position error accumulation. This implies that the relay agent may have to service each explorer frequently. However, if the explore dynamics can be accurately estimated, then the rate of position error accumulation can be decreased and made to primarily depend on the magnitude of external perturbations. A smaller position error growth rate implies more accurate open-loop navigation by each explorer, better explorer locating by the relay agent, and less frequent explorer servicing.

We approximate the uncertain dynamics of each explorer with an RNN, where ICL is used to improve the approximation of the explorer dynamics. The ICL strategy requires the collection of position data to promote learning [22]. Hence, the relay agent will linger with each explorer after the initial servicing instance to collect position data, where the lingering time will be selected in a manner that does not violate the subsequently defined maximum dwell-time condition of any explorer [see (34)]. Once the finite excitation condition [see (18)] is satisfied for an explorer, lingering for that explorer is no longer required and the unknown dynamics can be better estimated. The benefit of this strategy, as opposed to a robust control approach, is summarized in Remark 10, where the conservative error bounds generated prior to the satisfaction of the finite excitation condition in (18) can be relaxed and yield enhanced performance.

To quantify these objectives, four error systems are defined. The position tracking error of explorer $i \in F$ is

$$e_i \triangleq p_d - p_i \in \mathbb{R}^m. \tag{3}$$

The position estimation error of explorer i is

$$e_{1,i} \triangleq \hat{p}_i - p_i \in \mathbb{R}^m, \tag{4}$$

[1] The subsequent development can be extended to consider different goal locations.

where $\hat{p}_i \in \mathbb{R}^m$ denotes the position estimate of explorer i. The error between the desired position and the estimated position of explorer i is

$$e_{2,i} \triangleq p_d - \hat{p}_i \in \mathbb{R}^m. \tag{5}$$

The error between the estimated position of explorer i and the position of the relay agent is

$$e_{3,i} \triangleq \hat{p}_i - p_0 \in \mathbb{R}^m. \tag{6}$$

Combining (3)–(5) yields

$$e_i = e_{2,i} + e_{1,i}. \tag{7}$$

Let $R_{\text{com}} \in \mathbb{R}_{>0}$ denote the communication radius of the relay agent. When $\|p_0 - p_i\| \leq R_{\text{com}}$, the relay agent services explorer i, and p_i is measurable by both the relay agent and explorer i. When $\|p_0 - p_i\| > R_{\text{com}}$, explorer i is not serviced, and p_i is not measurable by any agent. As a result, the closed-loop dynamics of explorer i can be modeled as a switched system with two modes. Let the piecewise constant switching signal $\sigma_i : [0, \infty) \to \{S, U\}$ define the mode of the ith explorer, where S and U denote *serviced* and *unserviced*, respectively. Note that p_i is measurable when $\sigma_i = S$, and p_i is unmeasurable when $\sigma_i = U$. Since a single relay agent must service N explorers, the closed-loop dynamics of the relay agent can be modeled as a switched system with N modes. Consequently, let the piecewise constant switching signal $\sigma_0 : [0, \infty) \to F$ dictate the explorer the relay agent must service. The switching signal σ_0 determines the active mode of the relay agent. The value of σ_0 does not prevent the relay agent from providing position information to other explorers as the relay agent maneuvers toward the assigned explorer. In such a case, the opportunistic provision of position information to explorers different from the one assigned by the relay agent's switching signal is not captured by σ_0. Nevertheless, the relay agent can be made to ignore explorers that are encountered as the relay agent maneuvers toward the assigned explorer. Either strategy will achieve the consensus objective provided the subsequent maximum dwell-time condition of each explorer is always satisfied. At the initial time and for each $i \in F$, explorer i is provided with their position in the same global coordinate frame and is unserviced, i.e., $\sigma_i(0) = U$.

V. Control and State Estimate Development

Since a single relay agent is required to switch between multiple explorers, a maximum dwell-time condition is developed to ensure adequate predictor-based locating. When $\sigma_i = U$, the error in (4) of explorer i is allowed to increase to a user-defined threshold. To prevent (4) from growing beyond the desired threshold, the relay agent provides state (i.e., position) information to explorer i at an appropriate time; thus, resetting (4) when $\sigma_i = S$. The time at which the relay agent must service explorer i is determined by the subsequently developed maximum dwell-time condition. The dwell-time refers to the longest allowable time an explorer can go without position feedback, i.e., "move unattended." The intermittent provision of state information by the relay agent to explorer i when $\sigma_i = S$ results in the use of a reset map that introduces discontinuities in (4)–(6).

We now develop an adaptive update law for an RNN that approximates the unknown nonlinear dynamics of explorer i, where ICL is used to asymptotically improve an estimate of the unknown dynamics of explorer i. While alternative learning strategies can be considered, such as Gaussian processes, we chose to conduct learning via single-layer RNNs with ICL since we model and analyze the relay–explorer consensus problem from the perspective of deterministic systems. Because ICL requires samples of p_i, which are only available when $\sigma_i = S$, the relay agent will stay (linger) with explorer i for a time period. The effect from the combined use of a reset map, maximum dwell-time condition, and lingering time results in alternating periods where $\sigma_i = U$ and $\sigma_i = S$. To facilitate the subsequent switched systems analysis, let $t_{n,i}^U \in \mathbb{R}_{\geq 0}$ and $t_{n,i}^S \in \mathbb{R}_{\geq 0}$ denote the time of the nth instant the relay agent last serviced and starts servicing explorer i, respectively.[2] In general, $\sigma_i(t) = U$ during $t \in (t_{n,i}^U, t_{n,i}^S)$ and $\sigma_i(t) = S$ during $t \in [t_{n,i}^S, t_{n+1,i}^U]$ for each $n \in \mathbb{Z}_{\geq 0}$. Moreover, let $t_{n,i}^R \in \mathbb{R}_{\geq 0}$ denote the nth instant the relay agent initiates its return to explorer i, where $t_{n,i}^R \in (t_{n,i}^U, t_{n,i}^S]$ for each $n \in \mathbb{Z}_{\geq 0}$.

Consider a user-defined radius $R_{\max} > 2\sqrt{2}R_{\text{com}}$, and let $\mathcal{D} \triangleq \{\eta \in \mathbb{R}^m : \|\eta\| \leq R_{\max}\}$ denote the workspace in which the trajectory of each explorer evolves.[3] Note that $\mathcal{D}$ can be made arbitrarily large through the selection of $R_{\max}$. Given the compact set $\mathcal{D}$, the Stone–Weierstrass Theorem in [23, Th. 7.26] is leveraged to approximate the uncertain nonlinear dynamics of explorer i with an RNN over $\mathcal{D}$ such that

$$f_i(p_i) = W_i^\top \phi(p_i) + \varepsilon_i(p_i), \tag{8}$$

where $W_i \in \mathbb{R}^{L\times m}$ is an unknown constant weight matrix, $\phi : \mathbb{R}^m \to \mathbb{R}^L$ is a function composed of continuous and bounded basis functions, $L \in \mathbb{Z}_{>0}$ is the number of nodes used in the RNN, and $\varepsilon_i : \mathbb{R}^m \to \mathbb{R}^m$ denotes the bounded function reconstruction error [24, Sec. 1.1.3]. By substituting (8) into (1), the dynamics of explorer i can be expressed as

$$\dot{p}_i = W_i^\top \phi(p_i) + u_i + \varepsilon_i(p_i) + d_i. \tag{9}$$

The state estimate of explorer $i \in F$, which is synchronized between explorer i and the relay agent, evolves according to

$$\dot{\hat{p}}_i = \widehat{W}_i^\top \phi(\hat{p}_i) + u_i, \ \sigma_i = U \tag{10}$$

$$\hat{p}_i = p_i, \ \sigma_i = S, \tag{11}$$

where $\widehat{W}_i \in \mathbb{R}^{L\times m}$ denotes the estimate of the unknown weight matrix W_i, and the state estimate $\hat{p}_i$ is initialized as $\hat{p}_i(0) = p_i(0)$. The error between the unknown and estimated RNN weights is

$$\widetilde{W}_i \triangleq W_i - \widehat{W}_i \in \mathbb{R}^{L\times m}. \tag{12}$$

[2]The counting index n is unique to explorer i, and each explorer has their own index "n". This can be precisely expressed by writing $t_{n_i,i}^U$. However, we employ a slight abuse of notation by writing $t_{n,i}^U$ instead to facilitate readability. An analogous comment follows for $t_{n,i}^S$.

[3]The requirement that $R_{\max} > 2\sqrt{2}R_{\text{com}}$ comes from the development in Remark 7.

Based on the subsequent stability analysis, the controller for explorer i is

$$u_i \triangleq k_{1,i}e_{2,i} + k_{2,i}\mathrm{sgn}\left(e_{2,i}\right), \tag{13}$$

where $k_{1,i}, k_{2,i} \in \mathbb{R}_{>0}$ are selectable constants. Since p_d and $\hat{p}_i$ are known by the relay agent, u_i is known by the relay agent as well. The controller for the relay agent is

$$u_0 \triangleq \widehat{W}_i^\top \phi\left(\hat{p}_i\right) + u_i + k_3 e_{3,i} + k_4\mathrm{sgn}\left(e_{3,i}\right), \tag{14}$$

where $k_3 \in \mathbb{R}_{>0}$ is a piecewise constant parameter, $k_4 \in \mathbb{R}_{>0}$ is a selectable constant, and the subscript i reflects the current value of the switching signal σ_0, e.g., $\sigma_0(t) = i$.

The weight estimate $\widehat{W}_i$ in (10) is updated by an ICL-based adaptation law, which is only implemented after an excitation condition is satisfied. Let $t_{j,i} \in \bigcup_{n\in\mathbb{Z}_{\geq 0}}[t^S_{n,i}, t^U_{n+1,i}]$ denote the jth instant position information of explorer i is collected by the relay agent, which only occurs when $\sigma_i = S$. Moreover, let

$$x_i\left(t_{j,i}\right) \triangleq \begin{cases} 0_m, & t_{j,i} < \Delta t_i \\ p_i\left(t_{j,i}\right) - p_i\left(t_{j,i} - \Delta t_i\right) \\ \quad - \int_{t_{j,i}-\Delta t_i}^{t_{j,i}} u_i\left(\tau\right)\mathrm{d}\tau, & t_{j,i} \geq \Delta t_i, \end{cases} \tag{15}$$

where $\Delta t_i \in \mathbb{R}_{>0}$ is a user-defined integration window, and

$$y_i\left(t_{j,i}\right) \triangleq \begin{cases} 0_L, & t_{j,i} < \Delta t_i \\ \int_{t_{j,i}-\Delta t_i}^{t_{j,i}} \phi\left(p_i\left(\tau\right)\right)\mathrm{d}\tau, & t_{j,i} \geq \Delta t_i \end{cases} \tag{16}$$

denotes the known regressor of explorer i. Using (9) and (16) allows (15) to be expressed as

$$x_i\left(t_{j,i}\right) = \begin{cases} 0_m, & t_{j,i} < \Delta t_i \\ W_i^\top y_i\left(t_{j,i}\right) + h_i\left(t_{j,i}\right), & t_{j,i} \geq \Delta t_i, \end{cases} \tag{17}$$

$$h_i\left(t_{j,i}\right) \triangleq \int_{t_{j,i}-\Delta t_i}^{t_{j,i}} \left(\varepsilon_i\left(p_i\left(\tau\right)\right) + d_i\left(\tau\right)\right)\mathrm{d}\tau,$$

which is a useful expression that facilitates the stability analysis. Recording $M > L$ sample regressors $y_i(t_{j,i})$, a history stack (i.e., a data table) of regressors can be collected. For each $i \in F$, a finite time $T_i > 0$ is assumed to exist (see [22] and [25]) such that

$$\lambda_{\min}\left\{\sum_{j\in[M]} y_i\left(t_{j,i}\right) y_i\left(t_{j,i}\right)^\top\right\} > \lambda_i^* \tag{18}$$

for all $t \geq T_i$, where $\lambda_i^* \in \mathbb{R}_{>0}$ is a user-defined constant and $M \in \mathbb{Z}_{>0}$.[4] The time T_i denotes the instant when sufficient information about explorer i has been collected to enable asymptotic learning of its uncertain nonlinear dynamics. The RNN weight update law of explorer i, which is embedded within the continuous projection operator denoted by $\mathrm{proj}(\cdot,\cdot)$ and defined in [26, eq. 4], is designed as[5]

$$\dot{\omega}_i = \begin{cases} 0_{Lm}, & t \in [0, T_i), \\ \mathrm{proj}\left(\mu_i, \omega_i\right), & t \in [T_i, \infty), \end{cases} \tag{19}$$

where $\omega_i \triangleq \mathrm{vec}(\widehat{W}_i)$, $\mu_i \triangleq \mathrm{vec}(G_i)$, and $k_{\mathrm{ICL},i} \in \mathbb{R}_{>0}$ is a user-defined parameter, and[6]

$$G_i \triangleq k_{\mathrm{ICL},i} \sum_{j\in[M]} y_i(t_{j,i})(x_i^\top(t_{j,i}) - y_i^\top(t_{j,i})\widehat{W}_i) \tag{20}$$

denotes the ICL term. Note that G_i is piecewise continuous. Using (16) and (17), (20) can be expressed as

$$G_i = k_{\mathrm{ICL},i} \sum_{j\in[M]} y_i(t_{j,i})(y_i^\top(t_{j,i})\widetilde{W}_i + h_i^\top(t_{j,i})), \tag{21}$$

where $t_{j,i} \geq \Delta t_i$. Equation (21) shows that ICL injects the weight estimation error into the closed-loop dynamics of $\widetilde{W}_i$ in (12), where $\mathrm{vec}(\dot{\widetilde{W}}_i) = -\dot{\omega}_i$. The algorithm in Appendix C provides an implementation of the relay–explorer control strategy. For demonstration purposes, the switching signal used by the relay agent to service explorers is cyclical. Other switching signals can be employed provided they satisfy the maximum dwell-time condition for each explorer. In addition, the unknown explorer dynamics are used in the algorithm only to propagate the explorer positions forward in time. In practice, the relay agent would measure such positions when appropriate.

Remark 2: For every explorer $i \in F$, both explorer i and the relay agent have a copy of the $\hat{p}_i$ dynamics in (10), initial condition $\hat{p}_i(0)$, $\widehat{W}_i$ dynamics in (19), and initial condition $\widehat{W}_i(0)$. By numerically integrating the $\hat{p}_i$ dynamics and the $\widehat{W}_i$ dynamics under synchronized clocks and identical initial conditions, both explorer i and the relay agent will compute identical trajectories for $\hat{p}_i$ and $\widehat{W}_i$. In this way, both explorer i and the relay agent can know the unique $\hat{p}_i(t)$ and $\widehat{W}_i(t)$ for each time t without having to communicate, i.e., during an unserviced time interval. Clock synchronization for each pairing between the relay agent and explorer i, $i \in F$, can be achieved using results, such as [27] or [28], which provide distributed techniques for aligning virtual clocks in the presence of time delays and clock synchronization errors. During a servicing interval, $\hat{p}_i$ is reset to p_i and $\widehat{W}_i$ is updated according to (19). These values can be communicated during a servicing interval to preserve the synchronization of $\hat{p}_i$ and $\widehat{W}_i$. The final values of $\hat{p}_i$ and $\widehat{W}_i$ during a servicing interval serve as the initial conditions for the dynamics that will be numerically integrated during an unserviced interval. Also, the data in (20) are constant during unserviced intervals and can be communicated between explorer i and the relay agent during the final moments of the serviced interval to ensure synchronization.

The relevant closed-loop systems are now derived. Due to the reset of $\hat{p}_i$ in (11), the time derivatives of $e_{1,i}$, $e_{2,i}$, and $e_{3,i}$ do not exist everywhere. Substituting (7), (9), and (13) into the time derivative of (3) yields

$$\begin{aligned} \dot{e}_i = & -W_i^\top \phi\left(p_i\right) - k_{1,i}e_i + k_{1,i}e_{1,i} - k_{2,i}\mathrm{sgn}\left(e_{2,i}\right) \\ & - \varepsilon_i\left(p_i\right) - d_i. \end{aligned} \tag{22}$$

[4] T_i is unknown *a priori*, but the time when (18) becomes true can be measured. The condition in (18) reflects the collection of sufficient data to enable system estimation of the initially unknown nonlinear dynamics of explorer i.

[5] The projection operator is used to ensure that $\widehat{W}_i(t)$ remains within $\Omega = \{\omega \in \mathbb{R}^{L\times m} : \|\omega\| \leq \bar{\omega}\}$ for all $t \geq 0$, where $\bar{\omega} > 0$ is a user-defined parameter.

[6] Recall that $\mathrm{vec}(\cdot)$ denotes the vectorization transformation defined in Section II.

Substituting (9)–(11) into the time derivative of (4) yields

$$\dot{e}_{1,i} = \begin{cases} \widehat{W}_i^\top \phi(\hat{p}_i) - W_i^\top \phi(p_i) - \varepsilon_i(p_i) - d_i, & \sigma_i = U \\ 0_m, & \sigma_i = S. \end{cases} \tag{23}$$

Substituting (9)–(11) and (13) into the time derivative of (5) yields

$$\dot{e}_{2,i} = \begin{cases} -\widehat{W}_i^\top \phi(\hat{p}_i) - k_{1,i}e_{2,i} - k_{2,i}\mathrm{sgn}(e_{2,i}), & \sigma_i = U \\ -W_i^\top \phi(p_i) - k_{1,i}e_{2,i} - k_{2,i}\mathrm{sgn}(e_{2,i}) & \\ \quad -\varepsilon_i(p_i) - d_i, & \sigma_i = S. \end{cases} \tag{24}$$

Similarly, substituting (2), (9), (10), (13), and (14) into the time derivative of (6) yields

$$\dot{e}_{3,i} = \begin{cases} -k_3 e_{3,i} - k_4 \mathrm{sgn}(e_{3,i}), & \sigma_i = U \\ \widetilde{W}_i^\top \phi(p_i) - k_3 e_{3,i} - k_4 \mathrm{sgn}(e_{3,i}) & \\ \quad +\varepsilon_i(p_i) + d_i, & \sigma_i = S. \end{cases} \tag{25}$$

For explorer $i \in F$, let $\Lambda_i \triangleq \sum_{j\in[M]} y_i(t_{j,i}) y_i^\top(t_{j,i}) \in \mathbb{R}^{L\times L}$ and κ_i, γ_i be indicator functions, such that

$$\kappa_i \triangleq \begin{cases} 0, & \lambda_{\min}\{\Lambda_i\} \le \lambda_i^*, \\ 1, & \lambda_{\min}\{\Lambda_i\} > \lambda_i^*, \end{cases} \quad \gamma_i \triangleq \begin{cases} 0, & \sigma_i = U \\ 1, & \sigma_i = S. \end{cases}$$

Furthermore, let $\psi_i \triangleq [e_i^\top, p_0^\top, \hat{p}_i^\top, \omega_i^\top, \theta]^\top \in \mathbb{R}^{3m+Lm+1}$ be an auxiliary state vector for explorer i, where $\theta \in \mathbb{R}_{\ge 0}$ is a timer variable that evolves according to $\dot{\theta} = 1$ with $\theta(0) = 0$. Using the indicator functions κ_i and γ_i, the timer θ, (2), (9)–(11), (14), (19), (20), and (22), the closed-loop system for the auxiliary state of explorer i is $\dot{\psi}_i = H_i(\psi_i)$, such that

$$H_i(\psi_i) \triangleq \begin{bmatrix} -W_i^\top \phi(p_i) + \mathtt{a}_i - \varepsilon_i(p_i) - d_i(\theta) \\ \widehat{W}_i^\top \phi(\hat{p}_i) + u_i + k_3 e_{3,i} + k_4 \mathrm{sgn}(e_{3,i}) \\ \mathtt{b}_i \\ \kappa_i \mathrm{proj}(\mathrm{vec}(G_i(\psi_i)), \omega_i) \\ 1 \end{bmatrix}$$

$$\begin{aligned} \mathtt{a}_i &\triangleq -k_{1,i}e_i + k_{1,i}e_{1,i} - k_{2,i}\mathrm{sgn}(e_{2,i}), \\ \mathtt{b}_i &\triangleq \gamma_i(W_i^\top \phi(p_i) + u_i + \varepsilon_i(p_i) + d_i(\theta)) \\ &\quad + (1-\gamma_i)(\widehat{W}_i^\top \phi(\hat{p}_i) + u_i). \end{aligned} \tag{26}$$

Observe that the variables p_i, u_i, $e_{1,i}$, $e_{2,i}$, and $e_{3,i}$ can each be expressed as a function of ψ_i since $e_i = p_d - p_i$ and

$$(e_{1,i}, e_{2,i}, e_{3,i}) = \begin{cases} (\hat{p}_i - p_i, p_d - \hat{p}_i, \hat{p}_i - p_0), & \sigma_i = U, \\ (0_m, p_d - p_i, p_i - p_0), & \sigma_i = S. \end{cases} \tag{27}$$

Moreover, γ_i can also be expressed as a function of ψ_i, where each coordinate in (27) can be written as a single equation that switches based on the value of γ_i, similar to $\mathtt{b}_i$. Whenever $t = t_{n,i}^S$, for $n \in \mathbb{Z}_{\ge 0}$, the auxiliary state ψ_i jumps, that is, $\psi_i^+ = [e_i^\top, p_0^\top, p_i^\top, \omega_i^\top, \theta]^\top$, where ψ_i^+ denotes the value of ψ_i after a jump.

VI. Stability Analysis

To facilitate the stability analysis, we present the following auxiliary terms along with their corresponding bounds. Let

$$N_{1,i} \triangleq \widehat{W}_i^\top \phi(\hat{p}_i) - W_i^\top \phi(p_i) - \varepsilon_i(p_i) - d_i, \tag{28}$$

$$N_{2,i} \triangleq \widetilde{W}_i^\top \phi(p_i), \tag{29}$$

$$N_{3,i} \triangleq \sum_{j\in[M]} h_i^\top(t_{j,i}) \widetilde{W}_i^\top y_i(t_{j,i}), \tag{30}$$

$$N_{4,i} \triangleq \widehat{W}_i^\top \phi(\hat{p}_i), \tag{31}$$

$$N_{5,i} \triangleq \varepsilon_i(p_i) + d_i, \tag{32}$$

$$N_{6,i} \triangleq W_i^\top \phi(p_i). \tag{33}$$

Since $W_i \in \mathbb{R}^{L\times m}$ is a fixed matrix, $\widehat{W}_i$ is bounded through the use of the projection operator defined in [26], $\varepsilon_i(p_i)$ is bounded, as shown in [24, Sec. 1.1.3], d_i is bounded by assumption, ϕ is bounded by construction, Δt_i is a bounded user-defined integration window, $k_{\mathrm{ICL},i}$ is a user-defined parameter, $h_i(t_{j,i}) = \int_{t_{j,i}-\Delta t_i}^{t_{j,i}} (\varepsilon_i(p_i(\tau)) + d_i(\tau))\mathrm{d}\tau$ is bounded, and $y_i(t_{j,i}) = \int_{t_{j,i}-\Delta t_i}^{t_{j,i}} \phi(p_i(\tau))\mathrm{d}\tau$ is bounded, there exists a $c_{k,i} \in \mathbb{R}_{>0}$ such that $\|N_{k,i}(t)\| \le c_{k,i}$ for all $t \ge 0$ and for each $k = 1, 2, \ldots, 6$.

A. Explorer Agent Analysis

We begin the explorer analysis by first deriving a maximum dwell-time condition for each explorer $i \in F$ to ensure $\|e_{1,i}(t)\| \le V_T$ for all $t \in [t_{n,i}^U, t_{n,i}^S]$ and each $n \in \mathbb{Z}_{\ge 0}$. Since the relay agent maneuvers toward the estimated position of explorer i to enable servicing and the following theorem ensures $\|e_{1,i}(t)\| \le V_T$ for all $t \in [t_{n,i}^U, t_{n,i}^S]$ and each $n \in \mathbb{Z}_{\ge 0}$, the parameter V_T should be selected such that $V_T \in (0, R_{\mathrm{com}})$. Therefore, once the relay agent arrives at the estimated position of explorer i, explorer i will be within the communication radius of the relay agent, which ensures feasible servicing.

Theorem 3: If the relay agent services explorer i such that it satisfies the maximum dwell-time condition

$$t_{n,i}^S - t_{n,i}^U \le \frac{V_T}{c_{1,i}}, \tag{34}$$

then $\|e_{1,i}(t)\| \le V_T$ for all $t \in [t_{n,i}^U, t_{n,i}^S]$.

Proof: Let $V : \mathbb{R}^m \to \mathbb{R}_{\ge 0}$ be a common Lyapunov-like function, such that

$$V(e_{1,i}) \triangleq \frac{1}{2} e_{1,i}^\top e_{1,i}. \tag{35}$$

Using (23) when $\sigma_i = U$ and (28), the time derivative of (35) is

$$\dot{V}(e_{1,i}) = e_{1,i}^\top N_{1,i} \le c_{1,i}\|e_{1,i}\| \tag{36}$$

since $\|N_{1,i}\| \le c_{1,i}$. Substituting (35) into (36) yields

$$\dot{V}(e_{1,i}) \le c_{1,i}\sqrt{2V(e_{1,i})}. \tag{37}$$

Observe that $V(e_{1,i})$ and $\dot{V}(e_{1,i})$ are continuous, and, therefore, integrable, when $\sigma_i = U$. Integrating (37) over $[t_{n,i}^U, t_{n,i}^S]$, where $e_{1,i}(t_{n,i}^U) = e_{1,i}(t_{n,i}^S) = 0_m$, yields

$$V(e_{1,i}(t)) \le \frac{1}{2} c_{1,i}^2 \left(t - t_{n,i}^U\right)^2. \tag{38}$$

Integrating (37) over $(t_{n,i}^U, t_{n,i}^S)$ and $[t_{n,i}^U, t_{n,i}^S]$ yields no distinction since changing the value of the integrand at finitely many points does not change the value of the definite integral. Substituting (35) into (38) implies $\|e_{1,i}(t)\| \leq c_{1,i}(t - t_{n,i}^U)$ for all $t \in [t_{n,i}^U, t_{n,i}^S]$. Since $c_{1,i}(t - t_{n,i}^U)$ is an increasing function that bounds $\|e_{1,i}(t)\|$, we can ensure $\|e_{1,i}(t)\| \leq V_T$ over $[t_{n,i}^U, t_{n,i}^S]$ provided $c_{1,i}(t_{n,i}^S - t_{n,i}^U) \leq V_T$. Therefore, $c_{1,i}(t_{n,i}^S - t_{n,i}^U) \leq V_T$ yields the maximum dwell-time condition of explorer i in (34). ■

Remark 4: Recall that $\|e_{1,i}(t)\| = 0$ for all $t \in [t_{n,i}^S, t_{n+1,i}^U]$ and each $n \in \mathbb{Z}_{\geq 0}$. If the relay agent satisfies the maximum dwell-time condition in (34) for each $n \in \mathbb{Z}_{\geq 0}$, then $\|e_{1,i}(t)\| \leq V_T$ for all $t \geq 0$.

Remark 5: Given the maximum dwell-time condition in (34), the relay agent can linger and continuously service each explorer provided the lingering time does not violate the maximum dwell-time condition of other explorers. Let $\Delta t_i^L > 0$ denote the amount of time the relay agent lingers with explorer i. If the relay agent is to service explorer j after explorer i, then Δt_i^L must be selected such that $\Delta t_i^L < t_{q,j}^S - t_{q,j}^U$, where q denotes the imminent servicing instance of explorer j.

Recalling that $\mathcal{D} = \{\eta \in \mathbb{R}^m : \|\eta\| \leq R_{\max}\}$, the set of admissible initial conditions of (3) is

$$\mathcal{S}_\mathcal{D} \triangleq \left\{ \eta \in \mathbb{R}^m : \|\eta\| \leq \frac{\sqrt{2}}{2} R_{\max} \right\}.$$

The following theorem shows that $\mathcal{S}_\mathcal{D} \subset \mathcal{D}$ is forward invariant, which allows the RNN representation of $f_i|_\mathcal{D}$, i.e., the function f_i restricted to the domain $\mathcal{D}$, to hold throughout the execution of the consensus protocol.

Theorem 6: If the relay agent services explorer i such that it satisfies the maximum dwell-time condition in (34) for each $n \in \mathbb{Z}_{\geq 0}$, $e_i(0) \in \mathcal{S}_\mathcal{D}$, and $k_{1,i} > 0$, $k_{2,i} > 0$, and $V_T \in (0, R_{\text{com}})$ are selected such that

$$\frac{2\rho_i}{k_{1,i}} < \frac{\sqrt{2}}{2} R_{\max},$$

where $\rho_i \triangleq c_{5,i} + c_{6,i} + k_{1,i} V_T + k_{2,i}\sqrt{m} \in \mathbb{R}_{>0}$ and $m \in \mathbb{Z}_{>0}$ is the dimension of the position of explorer i, then the controller in (13) ensures the error system e_i in (3) is UUB in the sense that

$$\|e_i(t)\| \leq \frac{\rho_i}{k_{1,i}} \left(1 - e^{-k_{1,i} t}\right) + \|e_i(0)\| e^{-k_{1,i} t}. \tag{39}$$

In addition, $e_{2,i}$ is bounded, and the trajectories of $e_i(t)$ initialized inside $\mathcal{S}_\mathcal{D} \subset \mathcal{D}$ remain within $\mathcal{S}_\mathcal{D}$ for all $t \geq 0$.

Proof: Consider the common Lyapunov function candidate $V_1 : \mathbb{R}^{3m+Lm+1} \to \mathbb{R}_{\geq 0}$ defined as

$$V_1(\psi_i) \triangleq \frac{1}{2} e_i^\top e_i, \tag{40}$$

where ψ_i is the auxiliary state vector presented previously in (26). Suppose z_i is a Filippov solution to the differential inclusion $\dot{\psi}_i \in K[H_i](\psi_i)$ during flows, where z_i is reset according to $z_i^+ = [e_i^\top, p_0^\top, p_i^\top, \omega_i^\top, \theta]^\top$ after a jump. The mapping $K[\cdot]$ provides a calculus for computing Filippov's differential inclusion as defined in [29], and H_i is the vector field provided in (26). The time derivative of $V_1(\psi_i)$ exists almost everywhere (a.e.), and

$$\dot{V}_1(z_i) \overset{a.e.}{\in} \dot{\tilde{V}}_1(z_i), \tag{41}$$

where $\dot{\tilde{V}}_1(z_i)$ is the generalized time derivative of $V_1(z_i)$ along the Filippov trajectories of $\dot{z}_i = H_i(z_i)$. By [30, eq. 13],

$$\dot{\tilde{V}}_1(z_i) \triangleq \bigcap_{\xi \in \partial V_1(z_i)} \xi^\top \left[K[H_i]^\top (z_i), 1 \right]^\top,$$

where $\partial V_1(z_i)$ is the Clarke generalized gradient of $V_1(z_i)$. Since $V_1(z_i)$ is continuously differentiable in z_i during flows, $\partial V_1(z_i) = \{\nabla V_1(z_i)\}$, where ∇ denotes the gradient operator. Using the calculus of $K[\cdot]$ from [29] and simplifying the substitution of (22) into the generalized time derivative of (40) yields

$$\begin{aligned}\dot{\tilde{V}}_1(z_i) \subseteq & -\left\{ e_i^\top W_i^\top \phi(p_i) + k_{1,i} e_i^\top e_i + e_i^\top \varepsilon_i(p_i) + e_i^\top d_i \right\} \\ & - k_{2,i} e_i^\top K[\operatorname{sgn}(e_{2,i})] + k_{1,i} e_i^\top K[e_{1,i}].\end{aligned} \tag{42}$$

Using Young's inequality, $\|e_{1,i}\| \leq V_T$ from Theorem 3, (32), (33), (41), $\|N_{5,i}\| \leq c_{5,i}$, and $\|N_{6,i}\| \leq c_{6,i}$, the expression in (42) implies

$$\dot{V}_1(\psi_i) \overset{a.e.}{\leq} -k_{1,i} \|e_i\|^2 + \rho_i \|e_i\|. \tag{43}$$

Substituting (40) into (43) yields

$$\dot{V}_1(\psi_i) \overset{a.e.}{\leq} -2k_{1,i} V_1(\psi_i) + \rho_i \sqrt{2V_1(\psi_i)}. \tag{44}$$

Observe that $V_1(\psi_i)$ is continuous since e_i is a continuous function of time. Moreover, the time derivative of $V_1(\psi_i)$ along the Filippov solution $\psi_i = z_i$, i.e., $\dot{V}_1(z_i)$, is continuous almost everywhere. Therefore, both $V_1(\psi_i)$ and $\dot{V}_1(\psi_i)$ are integrable. Integrating (44) over $[0, t]$ and substituting (40) into the result yields (39), which implies e_i is UUB. From (43), we see that

$$\dot{V}_1(\psi_i) \overset{a.e.}{\leq} -\frac{k_{1,i}}{2} \|e_i\|^2, \quad \forall \|e_i\| \geq \frac{2\rho_i}{k_{1,i}}. \tag{45}$$

Consider the set $\mathcal{R} \triangleq \{\eta \in \mathbb{R}^m : \|\eta\| \geq 2\rho_i / k_{1,i}\}$, and recall the relation $2\rho_i / k_{1,i} < \sqrt{2} R_{\max}/2$. If $e_i \in \mathcal{S}_\mathcal{D} \cap \mathcal{R}$, then $\dot{V}_1(\psi_i) \overset{a.e.}{<} 0$ by (45). Conversely, if $e_i \in \mathcal{S}_\mathcal{D} \cap \mathcal{R}^C$, it then follows that $\dot{V}_1(\psi_i) \overset{a.e.}{\leq} -(k_{1,i}/2)\|e_i\|^2 + \rho_i \|e_i\|$, and $V_1(\psi_i)$ may grow. However, since $\mathcal{R}^C \subset \mathcal{S}_\mathcal{D}$, e_i will exit $\mathcal{R}^C$ before exiting $\mathcal{S}_\mathcal{D}$, and, therefore, flow into $\mathcal{S}_\mathcal{D} \cap \mathcal{R}$. Hence, initializing explorer i such that $e_i(0) \in \mathcal{S}_\mathcal{D}$ ensures $\mathcal{S}_\mathcal{D}$ is forward invariant for the error system e_i.

From (39), $e_i \in \mathcal{L}_\infty$. Since $e_i \in \mathcal{L}_\infty$ and $e_{1,i} \in \mathcal{L}_\infty$ by Theorem 3 and Remark 4, (7) implies $e_{2,i} \in \mathcal{L}_\infty$. Hence, (13) implies $u_i \in \mathcal{L}_\infty$. Since $e_{2,i} \in \mathcal{L}_\infty$ and p_d is fixed, $\hat{p}_i \in \mathcal{L}_\infty$. Finally, since $e_i \in \mathcal{L}_\infty$ and p_d is fixed, $p_i \in \mathcal{L}_\infty$. ■

Remark 7: If $R_{\max}$ is selected such that $R_{\max} > 2\sqrt{2} R_{\text{com}}$, which implies that $\sqrt{2} R_{\max} - 4R_{\text{com}} > 0$, then selecting

$$k_{1,i} > \frac{4\left(c_{5,i} + c_{6,i} + k_{2,i}\sqrt{m}\right)}{\sqrt{2} R_{\max} - 4R_{\text{com}}}$$

ensures $2\rho_i / k_{1,i} < \sqrt{2} R_{\max}/2$.

Corollary 8: For each $i \in F$, suppose the relay agent services explorer i such that it satisfies the maximum dwell-time condition in (34) for each servicing instant $n \in \mathbb{Z}_{\geq 0}$, $e_i(0) \in \mathcal{S}_\mathcal{D}$, $R_{\max} > \sqrt{2}R_{\text{com}}/2$, $V_T \in (0, R_{\text{com}}/4)$, $k_{2,i} \geq c_{5,i} + c_{6,i}$, $\varrho_i \triangleq 4(c_{5,i} + c_{6,i} + k_{2,i}\sqrt{m})$, and

$$k_{1,i} > \varrho_i \cdot \max\left\{\frac{1}{R_{\text{com}}}, \frac{1}{\sqrt{2}R_{\max} - R_{\text{com}}}\right\}. \quad (46)$$

If the relay agent is regulated to p_d once $\|e_i\| \leq 2\rho_i/k_{1,i}$ for every $i \in F$ and services all explorers continuously and simultaneously,[7] then the controller in (13) ensures that e_i in (3) is exponentially regulated for each $i \in F$.

Proof: Please see Appendix A. ■

The following theorem shows that $\widetilde{W}_i$ is constant for $t < T_i$ and UUB for $t \geq T_i$, which demonstrates the advantages afforded by the ICL strategy.

Theorem 9: If the relay agent services explorer i such that sufficient data are collected to satisfy (18), then the error system $\widetilde{W}_i$ in (12) is constant for all $t \in [0, T_i)$, i.e., $\widetilde{W}_i(t) = \widetilde{W}_i(0)$ over $[0, T_i)$, and UUB in the sense that

$$\begin{aligned}\|\text{vec}(\widetilde{W}_i(t))\|^2 \leq{}& \|\text{vec}(\widetilde{W}_i(T_i))\|^2 e^{-2k_{\text{ICL},i}\lambda_i^*(t-T_i)} \\ &+ \frac{c_{3,i}}{\lambda_i^*}\left(1 - e^{-2k_{\text{ICL},i}\lambda_i^*(t-T_i)}\right)\end{aligned} \quad (47)$$

for all $t \in [T_i, \infty)$.

Proof: Consider the common Lyapunov-like function $V_2 : \mathbb{R}^{Lm} \to \mathbb{R}_{\geq 0}$,

$$V_2(\text{vec}(\widetilde{W}_i)) \triangleq \frac{1}{2}\text{tr}(\widetilde{W}_i^\top \widetilde{W}_i). \quad (48)$$

Using $\widetilde{W}_i = W_i - \widehat{W}_i$ in (12) and $\omega_i = \text{vec}(\widehat{W}_i)$, the time derivative of (48) is

$$\dot{V}_2(\text{vec}(\widetilde{W}_i)) = \text{vec}(\widetilde{W}_i)^\top \text{vec}(\dot{\widetilde{W}}_i) = -\text{vec}(\widetilde{W}_i)^\top \dot{\omega}_i. \quad (49)$$

Case I: $t \in [0, T_i)$. Substituting (19) into (49) yields

$$\dot{V}_2(\text{vec}(\widetilde{W}_i)) = 0. \quad (50)$$

Hence, $V_2(\text{vec}(\widetilde{W}_i(t))) = V_2(\text{vec}(\widetilde{W}_i(0)))$ for all $t \in [0, T_i)$.
Case II: $t \in [T_i, \infty)$. Substituting (19) into (49) yields

$$\dot{V}_2(\text{vec}(\widetilde{W}_i)) = -\text{vec}(\widetilde{W}_i)^\top \text{proj}\,(\mu_i, \omega_i) \leq -\text{vec}(\widetilde{W}_i)^\top \mu_i, \quad (51)$$

where the inequality is due to [26, Prop. II]. Using (18) and (21), it follows that:

$$\begin{aligned}\dot{V}_2(\text{vec}(\widetilde{W}_i)) \leq{}& -k_{\text{ICL},i}\lambda_i^* \text{tr}(\widetilde{W}_i^\top \widetilde{W}_i) \\ &- k_{\text{ICL},i}\sum_{j\in[M]} h_i^\top(t_{j,i})\widetilde{W}_i^\top y_i(t_{j,i}).\end{aligned} \quad (52)$$

Recall that $|N_{3,i}| \leq c_{3,i}$. Substituting (30) and (48) into (52) yields

$$\dot{V}_2(\text{vec}(\widetilde{W}_i)) \leq -2k_{\text{ICL},i}\lambda_i^* V_2(\text{vec}(\widetilde{W}_i)) + k_{\text{ICL},i}c_{3,i}. \quad (53)$$

Observe that $V_2(\text{vec}(\widetilde{W}_i))$ is continuous by construction, and therefore, integrable over $[T_i, \infty)$. Since the discontinuities of $\dot{V}_2(\text{vec}(\widetilde{W}_i))$ are countable, because data are collected at discrete time instants to update G_i in (20), $\dot{V}_2(\text{vec}(\widetilde{W}_i))$ is integrable over $[T_i, \infty)$. Consequently,

$$\begin{aligned}V_2(\text{vec}(\widetilde{W}_i(t))) \leq{}& V_2(\text{vec}(\widetilde{W}_i(T_i)))e^{-2k_{\text{ICL},i}\lambda_i^*(t-T_i)} \\ &+ \frac{c_{3,i}}{2\lambda_i^*}\left(1 - e^{-2k_{\text{ICL},i}\lambda_i^*(t-T_i)}\right).\end{aligned} \quad (54)$$

Substituting $V_2(\text{vec}(\widetilde{W}_i)) = \|\text{vec}(\widetilde{W}_i)\|^2/2$ into (54) yields (47). ■

Remark 10: Once the finite excitation condition in (18) is satisfied, the model used in the predictor of explorer i will better approximate (asymptotically) the unknown dynamics given the bound in (47). Recall that $|N_{3,i}| \leq c_{3,i}$, where $N_{3,i} = \sum_{j\in[M]} h_i^\top(t_{j,i})\widetilde{W}_i^\top y_i(t_{j,i})$, and that a small $\|\text{vec}(\widetilde{W}_i)\|$ leads to be better model estimate. Since $|N_{3,i}|$ decreases as $\|\text{vec}(\widetilde{W}_i)\|$ decreases, and the parameter $c_{3,i}$ can be iteratively decreased as $\|\text{vec}(\widetilde{W}_i)\|$ decreases, one has: $\limsup_{t\to\infty}\|\text{vec}(\widetilde{W}_i(t))\|^2 = c_{3,i}/\lambda_i^*$. Note, further, that $c_{3,i}/\lambda_i^*$ can be reduced by collecting data that enable the selection of a larger λ_i^*. The maximum dwell-time in (34) is inversely proportional to the bound of $N_{1,i}$, i.e., $c_{1,i}$. Using (28), it can be shown that

$$\begin{aligned}\|N_{1,i}\| \leq{}& \|\widetilde{W}_i^\top \phi(\hat{p}_i)\| + \|\varepsilon_i(p_i)\| + \|d_i\| \\ &+ \|W_i\|\|\phi(\hat{p}_i) - \phi(p_i)\|,\end{aligned} \quad (55)$$

where $c_{1,i}$ can be selected larger than the maximum of the RHS of (55). Recall that the RHS of (55) is bounded by construction and the assumed bound on d_i. Once the finite excitation condition in (18) is satisfied for explorer i, the parameter $c_{1,i}$ can be iteratively decreased as $\|\text{vec}(\widetilde{W}_i)\|$ decreases. Therefore, the value of $c_{1,i}$ can be decreased after T_i, and the difference between consecutive servicing instances can be extended. Moreover, a smaller $c_{1,i}$ implies a slower error accumulation rate, as seen in (37), which yields more accurate open-loop navigation.

B. Relay Agent Analysis

When $t = 0$, the relay agent knows the initial position and corresponding maximum dwell-time condition for each explorer $i \in F$, where the future servicing time $t_{n,i}^S$ is computed at time $t_{n,i}^U$, i.e., the last instant explorer i is serviced. While various algorithms could be developed to determine which explorer the relay agent selects to service (e.g., [31], [32]), in this article, the relay agent selects the explorer associated with the smallest $t_{n,i}^S$.

Suppose the relay agent finished servicing explorer j at time $t_{m,j}^U$ and must maneuver, i.e., return, to explorer i for servicing. Then, the last servicing instant of explorer j is equal to the return time of explorer i, i.e., $t_{m,j}^U = t_{n,i}^R$, where $t_{n,i}^R \in (t_{n,i}^U, t_{n,i}^S]$.

[7] The simultaneous servicing of N explorers, once $\|e_i\| \leq 2\rho_i/k_{1,i}$ for each $i \in F$, can be treated as an additional mode of the relay agent. In such a case, the relay agent would have $N+1$ modes, which can be indicated by the switching signal $\sigma_o' : [0, \infty) \to F \cup \{N+1\}$, such that Mode $N+1$ corresponds to the simultaneous servicing of N explorers. Furthermore, the sufficient conditions of Corollary 8 imply that $2\rho_i/k_{1,i} < R_{\text{com}}$, enabling the simultaneous servicing of N explorers once the relay agent is regulated to p_d and $\|e_i\| \leq 2\rho_i/k_{1,i}$ for all $i \in F$.

If $\|p_0(t_{n,i}^R) - p_i(t_{n,i}^R)\| \leq R_{\text{com}}$, then the relay agent can immediately service explorer i; otherwise, the relay agent must maneuver toward the estimated position of explorer i, where the relay agent has $t_{n,i}^S - t_{n,i}^R > 0$ time units to reach explorer i's position estimate to enable servicing. The following theorem provides a sufficient gain condition to enable timely servicing by the relay agent.

Theorem 11: If $\|p_0(t_{n,i}^R) - p_i(t_{n,i}^R)\| > R_{\text{com}}$, then the state estimate update law in (10), controllers in (13) and (14), and RNN weight update law in (19) ensure the error system in (6) is exponentially regulated over $[t_{n,i}^R, t_{n,i}^S]$ and $[t_{n,i}^S, t_{n+1,i}^U]$, for each $n \in \mathbb{Z}_{\geq 0}$, provided $V_T \in (0, R_{\text{com}})$

$$k_3 \geq \frac{1}{t_{n,i}^S - t_{n,i}^R} \ln\left(\frac{\left\|e_{3,i}\left(t_{n,i}^R\right)\right\|}{R_{\text{com}} - V_T}\right), \tag{56}$$

where k_3 is piecewise constant, and $k_4 \geq c_{2,i} + c_{5,i}$.

Proof: Consider the common Lyapunov function candidate $V_3 : \mathbb{R}^{3m+Lm+1} \to \mathbb{R}_{\geq 0}$

$$V_3\left(\psi_i\right) \triangleq \frac{1}{2} e_{3,i}^\top e_{3,i}. \tag{57}$$

Suppose ζ_i is a Filippov solution to the differential inclusion $\dot{\psi}_i \in K[H_i](\psi_i)$ during flows, where ζ_i is reset according to $\zeta_i^+ = [e_i^\top, p_0^\top, p_i^\top, \omega_i^\top, \theta]^\top$ after a jump. The mapping $K[\cdot]$ provides a calculus for computing Filippov's differential inclusion, as defined in [29], and H_i is the vector field provided in (26). The time derivative of $V_3(\psi_i)$ exists almost everywhere, and

$$\dot{V}_3\left(\zeta_i\right) \overset{a.e.}{\in} \dot{\tilde{V}}_3\left(\zeta_i\right), \tag{58}$$

where $\dot{\tilde{V}}_3(\zeta_i)$ is the generalized time derivative of $V_3(\zeta_i)$ along the Filippov trajectories of $\dot{\zeta}_i = H_i(\zeta_i)$. By [30, eq. 13],

$$\dot{\tilde{V}}_3\left(\zeta_i\right) \triangleq \bigcap_{\xi \in \partial V_3\left(\zeta_i\right)} \xi^\top \left[K\left[H_i\right]^\top\left(\zeta_i\right), 1\right]^\top,$$

where $\partial V_3(\zeta_i)$ denotes the Clarke generalized gradient of $V_3(\zeta_i)$. Since $V_3(\zeta_i)$ is continuously differentiable in ζ_i during flows, $\partial V_3(\zeta_i) = \{\nabla V_3(\zeta_i)\}$. Using the calculus of $K[\cdot]$ from [29] and simplifying the substitution of (25) into the generalized time derivative of (57) yields

$$\dot{V}_3\left(\zeta_i\right) \subseteq -k_4 e_{3,i}^\top K\left[\operatorname{sgn}\left(e_{3,i}\right)\right] - k_3 e_{3,i}^\top K\left[e_{3,i}\right] \tag{59}$$

when $\sigma_i = U$, and

$$\begin{aligned}\dot{V}_3\left(\zeta_i\right) \subseteq &\left\{e_{3,i}^\top \widetilde{W}_i^\top \phi\left(p_i\right) + e_{3,i}^\top \varepsilon_i\left(p_i\right) + e_{3,i}^\top d_i\right\} \\ &- k_3 e_{3,i}^\top K\left[e_{3,i}\right] - k_4 e_{3,i}^\top K\left[\operatorname{sgn}\left(e_{3,i}\right)\right]\end{aligned} \tag{60}$$

when $\sigma_i = S$. Using (29), (32), (58), and $\|N_{k,i}\| \leq c_{k,i}$ for $k \in \{2, 5\}$, (59) implies

$$\dot{V}_3\left(\psi_i\right) \overset{a.e.}{\leq} -k_3\left\|e_{3,i}\right\|^2 - k_4\left\|e_{3,i}\right\| \tag{61}$$

when $\sigma_i = U$, and (60) implies

$$\dot{V}_3\left(\psi_i\right) \overset{a.e.}{\leq} -k_3\left\|e_{3,i}\right\|^2 - \left(k_4 - c_{2,i} - c_{5,i}\right)\left\|e_{3,i}\right\| \tag{62}$$

when $\sigma_i = S$. Since $k_4 \geq c_{2,i} + c_{5,i}$, (61) and (62) imply $\dot{V}_3(\psi_i) \overset{a.e.}{\leq} -k_3\|e_{3,i}\|^2$, where the use of (57) yields

$$\dot{V}_3\left(\psi_i\right) \overset{a.e.}{\leq} -2k_3 V_3\left(\psi_i\right). \tag{63}$$

Recall that, over $[t_{n,i}^R, t_{n+1,i}^U]$, the parameter k_3 is constant. Integrating (63) along the Filippov solution $\zeta_i = \psi_i$ over $[t_{n,i}^R, t_{n,i}^S]$ results in $V_3(\psi_i(t)) \leq V_3(\psi_i(t_{n,i}^R))e^{-2k_3(t - t_{n,i}^R)}$, where (57) implies

$$\|e_{3,i}(t)\| \leq \left\|e_{3,i}\left(t_{n,i}^R\right)\right\| e^{-k_3\left(t - t_{n,i}^R\right)} \tag{64}$$

over $[t_{n,i}^R, t_{n,i}^S]$. Similarly, $\|e_{3,i}(t)\| \leq \|e_{3,i}(t_{n,i}^S)\|e^{-k_3(t - t_{n,i}^S)}$ over $[t_{n,i}^S, t_{n+1,i}^U]$. Suppose the relay agent successfully serviced explorer i for each servicing event prior to n. By Theorem 3, $\|e_{1,i}(t)\| \leq V_T$ for all $t_{n,i}^S \geq t$. Observe that $\|p_0 - p_i\| \leq \|e_{3,i}\| + \|e_{1,i}\|$, where $\|p_0(t_{n,i}^S) - p_i(t_{n,i}^S)\| \leq R_{\text{com}}$ provided $\|e_{3,i}(t_{n,i}^S)\| + \|e_{1,i}(t_{n,i}^S)\| \leq R_{\text{com}}$. Since $\|e_{1,i}(t_{n,i}^S)\| \leq V_T < R_{\text{com}}$, servicing is achieved provided $\|e_{3,i}(t_{n,i}^S)\| \leq R_{\text{com}} - V_T$. Therefore, it is sufficient to ensure $\|e_{3,i}(t_{n,i}^R)\|e^{-k_3(t_{n,i}^S - t_{n,i}^R)} \leq R_{\text{com}} - V_T$, which implies that the relay agent can service explorer i at time $t_{n,i}^S$ provided (56) is satisfied. In addition, since $e_{3,i} = p_i - p_0$ when $\sigma_i = S$, the value of $e_{3,i}$ after a jump is bounded, i.e., $\|e_{3,i}^+\| \leq R_{\text{com}}$. Note that $u_0 \in \mathcal{L}_\infty$ over $[t_{n,i}^R, t_{n+1,i}^U]$ for each $n \in \mathbb{Z}_{\geq 0}$ since $u_i \in \mathcal{L}_\infty$ by the proof of Theorem 6, $\widehat{W}_i^\top \phi(\hat{p}_i)$ is bounded, and $e_{3,i} \in \mathcal{L}_\infty$ over each $[t_{n,i}^R, t_{n+1,i}^U]$. ■

Remark 12: From Theorems 3 and 6, $\|\hat{p}_i - p_i\| \leq V_T$ and $\|p_d - p_i\| \leq \sqrt{2}R_{\max}/2$ for all $t \geq 0$ and each $i \in F$, respectively. Hence, $\|p_d - \hat{p}_i\| \leq \sqrt{2}R_{\max}/2 + V_T$ for all $t \geq 0$ and each $i \in F$. Since the trajectories of all explorer position estimates are stable and the relay agent services each explorer by intermittently regulating its position to the position estimate of the corresponding explorer, it follows that the position of the relay agent is stable for all time. Moreover, the position of the relay agent converges toward p_d as all explorers converge to p_d in a UUB or exponential sense (see Theorem 6 and Corollary 8)

In practice, the relay agent will have a velocity limit, which may prevent the sufficient gain condition in (56) from being satisfied. This implies that there exists feasible servicing policies that are determined from the relay agent's velocity limit, the configuration of the explorers within the workspace, and the size of the workspace. While we reserve feasible policy synthesis for future work, the following proposition provides an upper bound on the piecewise constant gain of the relay agent.

Proposition 13: Suppose the conditions in Theorems 6 and 11 are satisfied, and the velocity of relay agent is bounded by $V_{0,\max} \in \mathbb{R}_{>0}$. If the relay agent is to service explorer i at time $t_{n,i}^S$ for some $n \in \mathbb{Z}_{\geq 0}$ and $\|e_{3,i}(t_{n,i}^R)\| > R_{\text{com}} - V_T$, then the piecewise constant gain of the relay agent is bounded in the sense that

$$k_{3,\max} \triangleq \frac{V_{0,\max} - \vartheta_i}{\left\|e_{3,i}\left(t_{n,i}^R\right)\right\|} \geq k_3(t) \tag{65}$$

for all $t \in [t_{n,i}^R, t_{n+1,i}^U]$, where $\vartheta_i \triangleq c_{4,i} + u_{i,\max} + k_4\sqrt{m} \in \mathbb{R}_{>0}$ and $\|u_i(t)\| \leq u_{i,\max}$ for all $t \geq 0$.

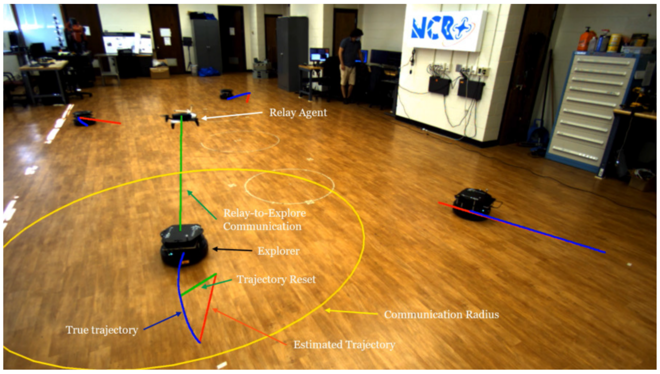

Fig. 1. Illustration of the relay–explorer consensus experiment. The four ground mobile robots represent the explorers, while the quadcopter represents the relay agent. The true and estimated position trajectories of each explorer are depicted by the blue and red lines, respectively, where the most recent 50 data points are shown. A green line connecting the true and estimated positions of an explorer corresponds to an initial servicing instance that causes the estimated position of the explorer to be reset to the corresponding true position. The yellow circle depicts the communication area of the relay agent, where any explorer within the yellow circle can be serviced by the relay agent (i.e., receive position feedback). A green line connecting the relay agent to an explorer represents the communication of position information from the relay agent to the explorer. It also represents the collection of explorer position information to facilitate model learning via ICL.

Proof: Please see Appendix B. ∎

VII. Experiment

In this section, we present the results of several experiments to verify the theoretical development and examine the performance of the relay–explorer consensus strategy.

A. Baseline Experiment

An experiment was conducted to investigate the performance of the theoretical development, where a video is available in [33]. A Parrot Bebop 2.0 quadcopter and four Clearpath Robotics Turtlebot 2 with a Kobuki base (ground mobile robots) are used for the relay agent and four explorers, respectively. A snapshot of the experiment is presented in Fig. 1.

The Turtlebot 2 features on-board wheel encoders and a gyroscope that are used to regulate the forward and angular velocity of the agent using a low-level control loop. A ground station running the Melodic Robotic Operating System with Ubuntu 16.04 is used to generate velocity commands for the five agents. The control commands are transmitted to the relay agent and four explorers through WiFi channels. The experiment was conducted in an approximately 8×5 m^2 testing space. A NaturalPoint, Inc., OptiTrack motion capture system is used to provide position information at 120 Hz. The standard deviations of linear position measurements and angular position measurements are approximately 1 cm and 1°, respectively. Position measurements from the motion capture system are continuously broadcast to the relay agent and broadcast to explorer i whenever $\|p_0 - p_i\| \leq R_{\text{com}}$, where these position measurements are expressed in terms of the same global coordinate frame. If multiple explorers are within R_{com} of the relay agent, then position information is sequentially broadcast to those

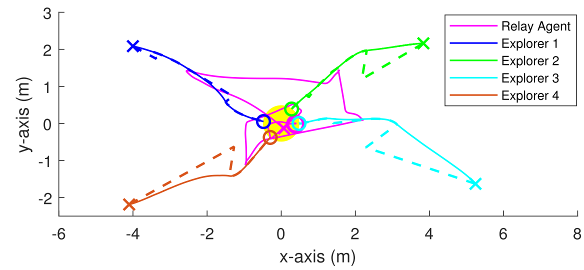

Fig. 2. Depiction of the true and estimated position trajectories of the MAS. The $\times$'s and $\circ$'s denote the initial and final positions of each agent, respectively. The solid paths represent the true position trajectories of the agents, whereas the dashed paths represent the estimated position trajectories of the explorers. Note that the control strategy does not employ a position estimate for the relay agent; hence, there is no dashed path for the relay agent.

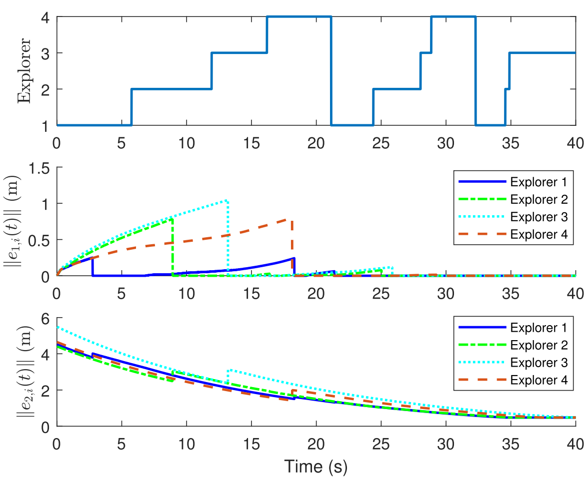

Fig. 3. Top plot shows the switching signal that the relay agent uses to determine which explorer to service. The middle plot shows the norm of the position estimation error for each explorer, which captures the difference between the estimated and true positions of the corresponding explorer. In particular, $\|e_{1,i}(t)\| \leq V_T$ for all $i \in F$ and all $t \geq 0$. The bottom plot shows the norm of the estimated position tracking error for each explorer, i.e., the mismatch between the goal and estimated positions.

explorers. For example, if $\|p_0 - p_q\| \leq R_{\text{com}}$ for $q = 1, 2, 3$, then Explorer 1 receives position feedback at one time instant, Explorer 2 receives position feedback the next time instant, etc. When $\|p_0 - p_i\| > R_{\text{com}}$, explorer i does not receive position measurements and uses the estimator in (10) to determine its position. Due to the nonholonomic dynamics of the Turtlebot 2, a PI controller was used to align the angular position of each explorer with the direction of the velocity vector commanded by the controller in (13). As a further source of uncertainty, the angular position was estimated when feedback was unavailable. Moreover, $0.07\sin(0.1t)$ was injected into the angular position estimate to better demonstrate the robustness of the developed control system. This disturbance was also employed to ensure the eventual disagreement between each explorer's true and estimated trajectories, and, therefore, necessitate servicing by the relay agent to achieve position consensus. The experimental results are presented in Figs. 2–7, and the parameters used to conduct the experiment are the following: $R_{\text{com}} = 1.5$ m, $V_{0,\max} = 2$ m/s, $k_{1,i} = 0.06, k_{2,i} = 0.01, k_4 = 0.01, k_{\text{ICL},i} = 1$ for each $i \in F$, the lingering time, i.e., Δt_i^L, is 3 s for each

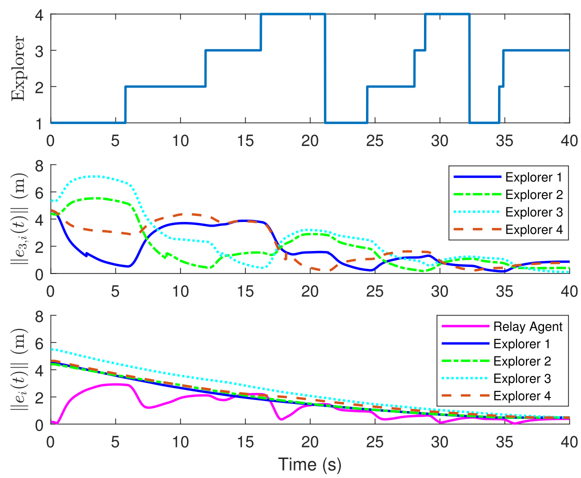

Fig. 4. Top plot shows the switching signal that the relay agent uses to determine which explorer to service. The middle plot shows the norm of the location errors, which measures the distance between the position of the relay agent and the estimated position of each explorer. The bottom plot shows the norm of the position tracking error of the relay agent and each explorer, i.e., the mismatch between the goal position and the true position for the respective agent.

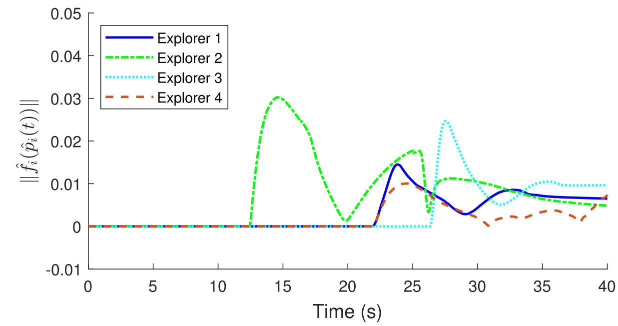

Fig. 5. Plot depicts the norm of the estimated nonlinear drift dynamics of each explorer. Note that $\hat{f}_i(\hat{p}_i) \triangleq \widehat{W}_i^\top \phi(\hat{p}_i)$ for each $i \in F$.

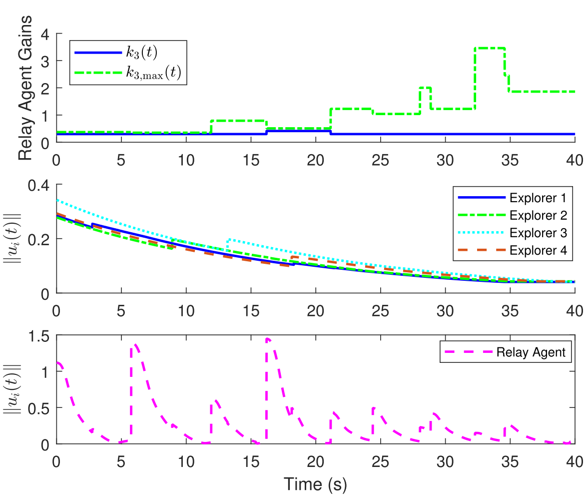

Fig. 6. Top plot depicts both the actual and maximum piecewise constant gain the relay agent used to service each explorer during the experiment. The middle plot shows the norm of the control signal for each explorer in the MAS. The bottom plot shows the norm of the control signal for the relay agent.

$i \in F$, the maximum dwell-time is 23 s for each $i \in F$, the number of nodes in the RNN of each explorer is 5, i.e., $L = 5$, $V_T = 0.85R_{\text{com}} = 1.275$ m, and the upper and lower bounds used in the projection algorithm are -0.5 and 0.5, respectively. Note that k_3 was initialized as 0.3 and subsequently modified as necessary according to the lower and upper bounds in (56) and (65), respectively. The RNN of each explorer used Gaussian radial basis functions with a standard deviation of 0.75 m. The radial basis functions were evenly spaced along a centering line defined between the goal location and the initial position of each explorer, where the perpendicular distance of the basis function center and the centering line was randomly selected from a normal distribution. The desired position was set to the origin, that is, $p_d = [0, 0]^\top$.

Fig. 2 shows the planar trajectories of each explorer's true and estimated position as well as the trajectory of the relay agent's position. Fig. 2 indicates that the consensus objective is achieved, where all agents reached the desired region.[8] Fig. 3 shows that $\|e_{1,i}(t)\| \leq V_T$ for all $t \geq 0$ and $i \in F$, i.e., the norm of the position estimation error is uniformly upper bounded by V_T for each explorer. This confirms the result of Theorem 3 since the switching signal (top plot in Fig. 3) that the relay agent uses to service each explorer was constructed to satisfy the maximum dwell-time condition in (34). In addition, the plot of $\|e_{2,i}\|$ versus time in Fig. 3 shows that $e_{2,i}$ is converging to 0_2 for each $i \in F$, where the deviation from 0 is due to the experiment being terminated to prevent collisions between explorers. Fig. 4 depicts the norm of the position tracking error for each explorer, which exponentially converges into a closed ball containing the origin. While this may seem like a UUB result, exponential regulation would have occurred if the ground mobile robots could all occupy the same space. Regardless, regulation of e_i to a neighborhood of the origin confirms Theorem 6 and Corollary 8. Let e_0 denote the position tracking error of the relay agent. Fig. 4 also demonstrates that e_0 is artificially UUB, which, in conjunction with the previous observation, shows that all explorers and the relay agent are driven into a closed ball containing p_d. In Fig. 5, the norm of the estimated drift dynamics are presented, where the initial weights of the RNN were set to 0 for each $i \in F$. Since the motion model of each ground mobile robot and the ideal weights of each RNN are unknown, no analytical comparison between the true and estimated explorer drift dynamics can be made. However, we provide a numerical comparison in the proceeding section. Fig. 6 demonstrates that the gain of the relay agent is uniformly upper bounded by $k_{3,\max}$, where the maximum steady state velocity of the relay agent was 1.15 m/s. Finally, Fig. 7 illustrates that the relay agent serviced each explorer in a manner that always satisfied the maximum dwell-time condition, which complements the observation that $\|e_{1,i}(t)\| \leq V_T$ for all $t \geq 0$ and $i \in F$ in Fig. 3.

[8] While the theoretical control strategy drives each agent to the desired position p_d, we terminate the experiment once the explorers are within a closed ball of radius 1.5 m centered at p_d to prevent collisions between the explorers.

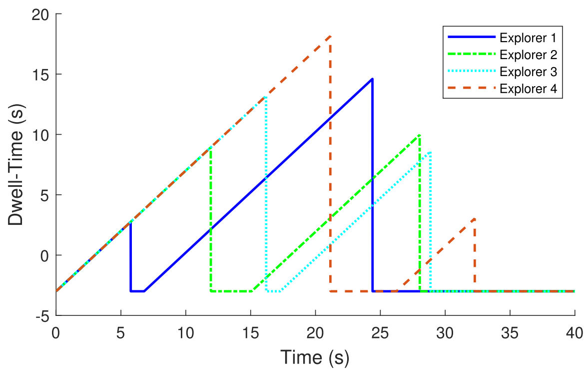

Fig. 7. Plot depicts the time intervals corresponding to when each explorer was serviced and unserviced. A linear increase corresponds to an unserviced time interval, whereas a flat region corresponds to a serviced time interval. The maximum dwell-time of all agents was 23 s, where the relay agent serviced each agent such that no explorer had an unserviced time interval longer than 23 s.

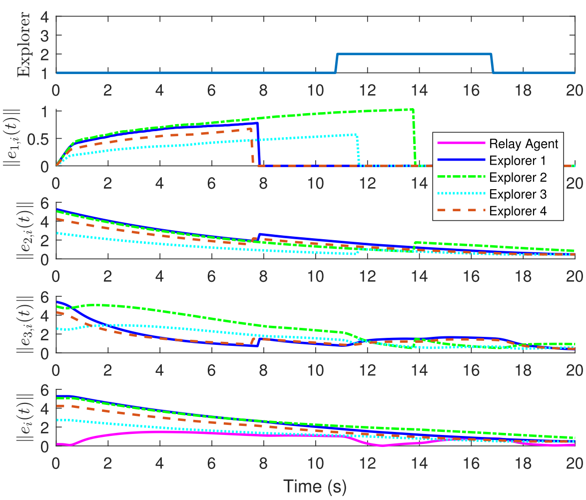

Fig. 8. Experimental results for a fast explorer speed and an aperiodic disturbance. The MAS achieved the consensus objective.

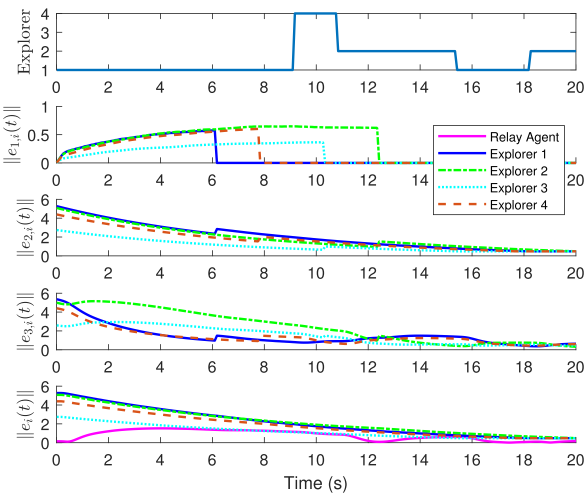

Fig. 9. Experimental results for a fast explorer speed and a periodic disturbance. The MAS achieved the consensus objective.

B. Comparative Experiments

In total, four additional experiments were conducted, where the speed of the explorers was set to either slow or fast, while the disturbance affecting the explorers was either aperiodic or periodic. A slow and fast explorer speed was achieved by setting $k_{1,i}$ in (13) to either 0.04 or 0.13, respectively, for each $i \in F$. An aperiodic disturbance means that d_i was set to a step input with a value of 0.4 rads/s when $t \in [3, 5]$ and a value of 0 rads/s, otherwise. A periodic disturbance means that $d_i(t) = 0.07 \sin(0.1t)$ rads/s. All other parameters used in these experiments are identical to those of the baseline experiment. For each comparative experiment, all explorers had the same value for $k_{1,i}$ and were affected by the same disturbance. The results of Experiments 1–4 are shown in Figs. 8–11, respectively.

In all four experiments, the MAS achieved the consensus objective. In the experiments with a fast explorer speed (see Figs. 8 and 9), the relay agent did not have the opportunity to individually visit each explorer for servicing, which is demonstrated by the switching signal subplot. However, because we employed opportunistic servicing, each explorer was serviced at least once as shown by the resets in the $\|e_{1,i}\|$ subplot in Figs. 8 and 9. Note that opportunistic servicing means that the relay agent provided position information to any explorer that was within communication range, even if the explorer was different from the one assigned by the switching signal σ_0. Moreover, the relay agent did not linger with an explorer different from the one assigned by the switching signal σ_0. In particular, the switching signal and $\|e_{1,i}\|$ subplots in Fig. 8 show that the relay agent was first assigned Explorer 1 for servicing. As the relay agent moved towards Explorer 1, the relay agent encountered Explorer 4. Hence, the relay agent opportunistically serviced Explorer 4 before servicing Explorer 1. Because the order of servicing is based on the opportunistic servicing strategy and the maximum dwell-time condition in (34), i.e., the explorer with the least amount of time left before its maximum dwell-time expires gets serviced next, and both Explorers 1 and 4 were recently serviced, the relay agent was assigned Explorer 2 for servicing. As the relay agent maneuvered towards Explorer 2, the relay agent encountered Explorer 3, which explains why Explorer 3 was opportunistically serviced before Explorer 2 was serviced. Once Explorer 2 had been serviced, all explorers were close enough to the goal region. Hence, the relay agent moved to p_d to facilitate the simultaneous servicing of all four explorers as shown by $\|e_{1,i}(t)\| = 0$ for all $t \geq 14$ and $i = 1, 2, 3, 4$.[9] In the experiments with a slow explorer speed (see Figs. 10 and 11), the relay agent individually visited each explorer to provide position feedback. In fact, the slow explorer speeds allowed the relay agent to individually visit each explorer multiple times as shown in the switching signal subplots in Figs. 10 and 11. In addition, in both the slow-speed and fast-speed experiments, the MAS was robust to a 2-s aperiodic disturbance that was an order of magnitude larger than the persistent periodic disturbance.

[9]Because a single relay agent must service N explorers, where N can be large, and each explorer has a maximum dwell-time condition that must be satisfied for all time, the relay agent may be unable to opportunistically service multiple explorers, especially if opportunistic servicing is performed sequentially. Therefore, future works may investigate the path planning problem for the relay agent to determine appropriate servicing strategies.

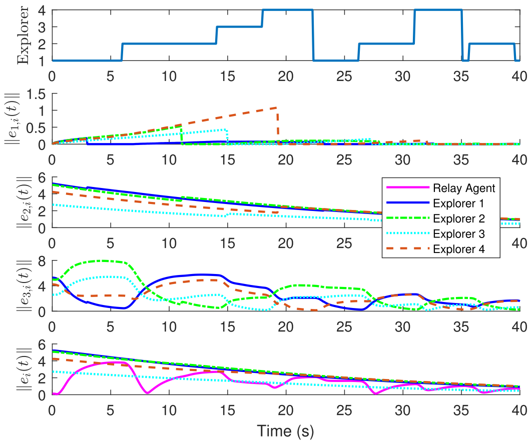

Fig. 10. Experimental results for a slow explorer speed and an aperiodic disturbance. The MAS achieved the consensus objective.

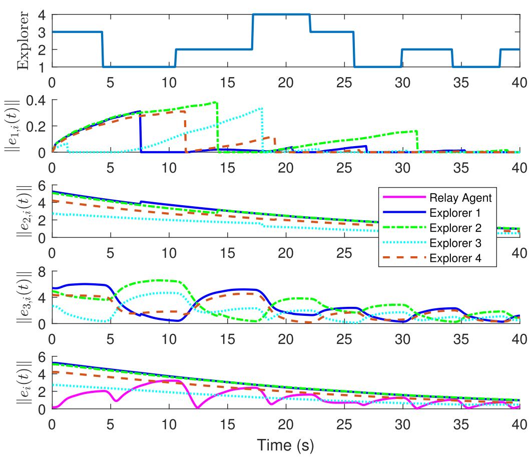

Fig. 11. Experimental results for a slow explorer speed and a periodic disturbance. The MAS achieved the consensus objective.

VIII. Simulation Examples

In this section, we present the results of several simulations to further verify the theoretical development, explore its scalability, and make comparisons with our previous work.

A. Baseline Simulation

Let $p_i \triangleq [p_{1,i}, p_{2,i}]^\top \in \mathbb{R}^2$ ($m = 2$), where $p_{1,i}$ and $p_{2,i}$ denote the first and second coordinates of the position vector of explore i, respectively. The motion model of explorer i is

$$\dot{p}_i = \begin{bmatrix} \beta_{1,i}\left(\sin\left(p_{1,i}\right)+1\right) \\ \beta_{2,i}\left(\cos\left(p_{2,i}\right)+1\right) \end{bmatrix} + u_i + d_i. \tag{66}$$

Observe that $\beta_{1,i}$ and $\beta_{2,i}$ are randomly chosen constants from a uniform distribution on [0.05,0.1]. The disturbance d_i is random and sampled from a uniform distribution on $[-10^{-3}, 10^{-3}]$ at every time step. Although the analysis is performed under the assumption of a continuous and bounded disturbance, we consider a random disturbance to evaluate the performance of the control strategy.[10] The magnitude of the disturbance was selected as 10^{-3} to ensure an approximate $10:1$ signal-to-noise ratio. Larger ratios can be considered, and while the control strategy may achieve the consensus objective under larger signal-to-noise ratios, the performance of the ICL strategy may degrade. The drift dynamics, i.e., $f_i(p_i) = [\beta_{1,i}(\sin(p_{1,i})+1), \beta_{2,i}(\cos(p_{2,i})+1)]^\top$, are unknown to the agents, but it is the goal of the relay agent to estimate these dynamics for every explorer by using the ICL strategy. From (20), if the relay agent communicates $\sum_{j\in[M]} y_i(t_{j,i})x_i^\top(t_{j,i})$ and $\sum_{j\in[M]} y_i(t_{j,i})y_i^\top(t_{j,i})$ to explorer i during each servicing event, then synchronous numerical integration of (10) and (19) by the relay agent and explorer i yields synchronized position estimates of explorer i for both agents.

The baseline case considers a five-agent system with four explorers ($N = 4$). The initial position of explorer i is given by $p_i(0) = [10\cos(2\pi(i-1)/N), 10\cos(2\pi(i-1)/N)]^\top$ for each $i \in F$. The desired consensus position is $p_d = [-3, -1]^\top$, and the initial position of the relay agent is $p_0(0) = [10, 10]^\top$. Each explorer estimates their position using an RNN with three neurons ($L = 3$). Recall that the estimated position of explorer i is generated using (10), where $\widehat{W}_i^\top \phi(\hat{p}_i)$ represents the estimated drift dynamics of explorer i. Since we require the relay agent's position estimate of explorer i to be synchronized with that of explorer i, the relay agent also uses a three-neuron RNN to estimate explorer i's position. The basis functions used in the RNN for explorer i are $\phi(\hat{p}_i) = [1, \sin(\hat{p}_{1,i}), \cos(\hat{p}_{2,i})]^\top$, where $\hat{p}_i \triangleq [\hat{p}_{1,i}, \hat{p}_{2,i}]^\top \in \mathbb{R}^2$ denotes the estimated position of explorer i. The communication radius of the relay agent is $R_{\text{com}} = 2$, and the controller gains for explorer i are $k_{1,i} = 0.25$ and $k_{2,i} = 0.15$ for all $i \in F$. For simplicity, the relay agent uses a cyclical switching signal to service each explorer. Hence, the sequence of servicing explorers is $1 \to 2 \to 3 \to 4 \to 1$. The parameter V_T is set to 1.9, which implies that $\|e_{1,i}\| \leq V_T$ for all time by Theorem 3 and Remark 4. Recall that V_T must be selected smaller than R_{com} so that the relay agent can service explorer i once the relay agent regulates its position to the estimated position of explorer i. The parameter $c_{1,i}$ is selected as 2.2 for all $i \in F$. Hence, the maximum dwell-time for each agent is $V_T/c_{1,i} = 0.864$. The lingering time Δt_i^L for explorer i is selected as 0.065, where the maximum step size of the simulation is 0.005. Consequently, the relay agent will have at least 13 time steps per servicing instance to collect data from each explorer. The k_3 control gain of the relay agent is selected according to (56), and $k_4 = 1$. The minimum eigenvalue used in (18) is $\lambda_i^* = 1.3$ for each $i \in F$. The ICL gain is $k_{\text{ICL},i} = 0.15$, and the length of the ICL integration window is $\Delta t_i = 0.052$ for each $i \in F$. With respect to the continuous projection operator in [26, eq. 4], $\theta_0 = 0.5$ and $\varepsilon = 0.5$, which ensure that $\|\widehat{W}_i(t)\| \leq 1$ for all $t \geq 0$ and each $i \in F$. This system was simulated in MATLAB using [34], where Figs. 12–15 illustrate the results.

With respect to Figs. 12 and 13, servicing by the relay agent enables the MAS to achieve the consensus objective. Fig. 14

[10]The disturbance can be upper bounded by a continuous bounded function of time, which can be used for analysis purposes. An example of such a bound is the constant function with magnitude 10^{-3}.

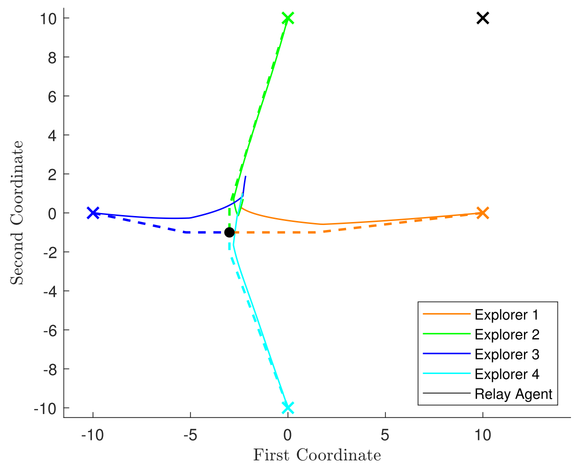

Fig. 12. Solid lines and dashed lines represent the position trajectories and estimated position trajectories of the explorers, respectively, when the relay agent does not service any explorer (the relay agent is stationary). The initial position of each agent is depicted by an $\times$. The desired consensus position is represented by the black dot. Observe that all explorers manage to approach the desired consensus position but eventually miss it entirely. The fourth explorer even passes by the desired consensus position but is unable to stop at p_d since it does not know its true position. The deviation of the explorers from p_d without servicing by the relay agent is worsened under more severe perturbations.

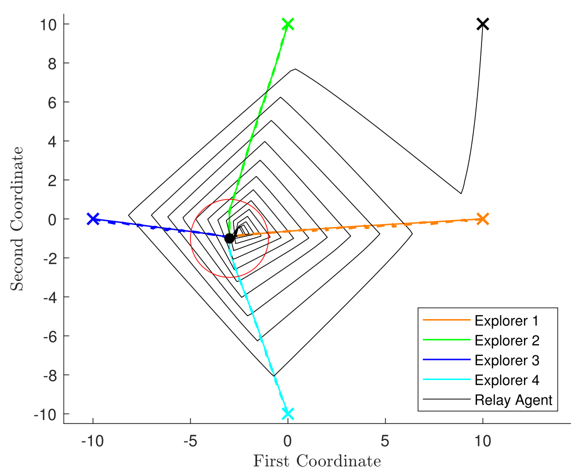

Fig. 13. Solid lines and dashed lines represent the position trajectories and estimated position trajectories of the explorers, respectively. The position trajectory of the relay agent is depicted by the black solid line. The initial position of each agent is illustrated by an $\times$. The desired consensus position is represented by the black dot. The red circle depicts the communication region of the relay agent once it is regulated to the desired consensus position. Note that the MAS achieves the consensus objective when the relay agent services each explorer as prescribed by the maximum dwell-time condition. Moreover, the rate of servicing enables each estimated trajectory to remain close to the corresponding true trajectory as shown by the closeness between corresponding solid and dashed lines. Recall that the communication radius of the relay agent is $R_{\text{com}} = 2$, and the servicing of explorer i occurs whenever $\|p_0 - p_i\| \leq R_{\text{com}}$. This implies that the relay agent will regulate its position to the estimated position of explorer i until $\|p_0 - p_i\| \leq R_{\text{com}}$. The relay agent then regulates its position to the true position of explorer i during the lingering portion of servicing. Because the lingering time is 0.065, the relay agent looks like it only visits an explorer and immediately leaves afterward to service another explorer. Consequently, the relay agent is always about 2 units away from an explorer when it is serviced. This implies that the position of the relay agent is driven to p_d as the explorers approach the ball of radius 2 centered at p_d, explaining why the relay agent travels to service the explorers when inside this ball.

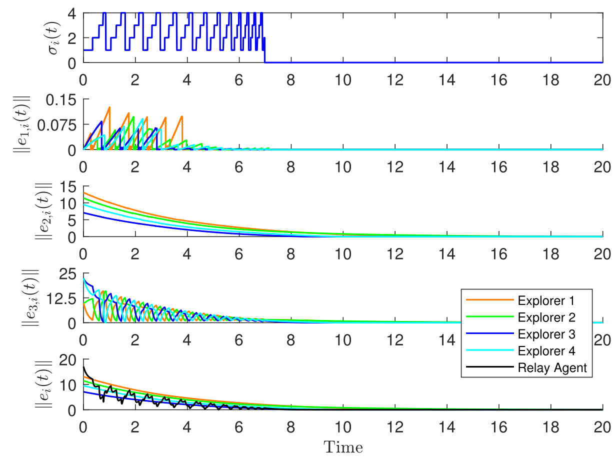

Fig. 14. Top plot shows the switching signal that the relay agent uses to service the explorers. Once the explorers are sufficiently close to p_d (see Corollary 8), the relay agent is regulated to p_d, where this is represented by $\sigma_0(t) = 0$ for $t > 7$. The second plot from the top shows the evolution of $\|e_{1,i}\|$ for each explorer, where $e_{1,i} = \hat{p}_i - p_i$ and $\|e_{1,i}(t)\| \leq V_T = 1.9$ for all $t \geq 0$ and $i \in F$. Thus, the estimated position trajectory of explorer i is always within a distance of R_{com} from the corresponding true position trajectory. The middle plot shows the evolution of $\|e_{2,i}\|$ for each explorer, which is exponentially driven to 0. Recall that $e_{2,i} = p_d - \hat{p}_i$; hence, the estimated positions of each explorer converge to p_d. The fourth plot from the top shows the $\|e_{3,i}\|$ versus time for each explorer. Each error can be bounded by a nonnegative exponentially decaying function of time since all explorer estimated positions converge to p_d. The bottom plot shows $\|e_i\|$ versus time for each agent, where e_i quantifies the mismatch between the true position of agent i and p_d for $i \in F \cup \{0\}$. The plot shows that the MAS is exponentially regulated to p_d, and, therefore, the consensus objective is achieved.

illustrates the switching signal and the evolution of the normed error signals for the simulation. We can confirm that $\|e_{1,i}(t)\| \leq V_T$ for all $t \geq 0$ and each $i \in F$, and each agent was exponentially regulated to p_d. For $t > 7$, the switching signal equals 0, which means that the relay agent was regulated to p_d so that it could service all explorers simultaneously using Mode $N + 1$. Fig. 15 demonstrates the results of the ICL estimation strategy. In this case, ICL enabled the relay agent to virtually identify the drift dynamics of each explorer. Recall that the RNN weights are updated only after the finite excitation condition in (18) is satisfied, which occurs before $t = 6$ for every explorer. Fig. 15 shows that the estimated explorer drift dynamics converge to a small neighborhood of the true drift dynamics moments after (18) is met for each explorer. Fig. 15 shows that the drift dynamics of all explorers are accurately estimated for $t \geq 6$. The effect of this model learning is that the estimated position closely matches the true position of each explorer as demonstrated by the small errors in $\|e_{1,i}(t)\|$ for $t \in [6, 7]$ in Fig. 14. Note that, during $t \in [6, 7]$, each explorer employs intermittent state feedback from the relay agent (through servicing) prior to continuous servicing by the relay agent due its regulation to p_d at time $t \approx 7$.

B. Scalability Study

We also conduct multiple simulations with a similar parameter configuration to investigate scalability of the developed control strategy. All models, parameters, and initial conditions are identical to the baseline case except for the number of

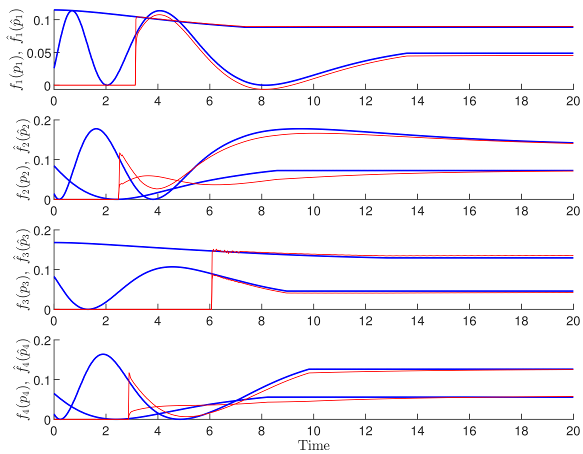

Fig. 15. Each plot shows the componentwise evolution of the true drift dynamics in blue and the corresponding estimated drift dynamics in red for an explorer. Since all RNN weights are initialized as zero and held constant until the finite excitation condition in (18) is satisfied, the initial estimated drift dynamics are zero. Once (18) is met, the estimated drift dynamics are updated and are shown to converge to a small neighborhood of the true drift dynamics. Recall that Theorem 9 states that $\widetilde{W}_i$ is UUB, where the ultimate bound is below 0.1 for each explorer in simulation.

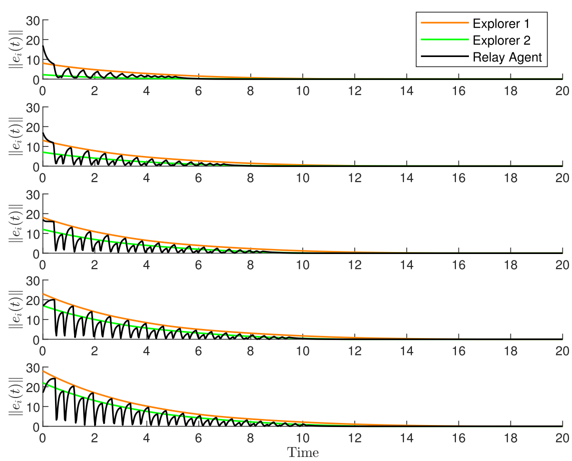

Fig. 16. Normed position tracking errors for 1 relay agent servicing 2 explores. The plots from top to bottom are in correspondence with $R = 5, 10, 15, 20, 25$. For each value of R, the consensus objective was achieved.

explorers and their initial positions. The disturbance d_i was also sampled from a uniform distribution on $[-10^{-1}, 10^{-1}]$ at every time step, and the ICL gain was changed to $k_{\mathrm{ICL},i} = 0.01$ for each $i \in F$. The initial position of explorer i is selected as $p_i(0) = R[\cos(2\pi(i-1)/N), \cos(2\pi(i-1)/N)]^\top$, where the variable R takes on the values 5, 10, 15, 20, and 25. Hence, given a fixed number of explorers, a simulation is performed for each value of $R \in \{5, 10, 15, 20, 25\}$. These types of initial positions are selected to ensure an unbiased comparison between simulations. We generate simulation results for 1 relay agent servicing 2, 3, 4, 5, and 6 explorers. Figs. 16–20 illustrate the results, which convey that the feasibility of the relay–explorer strategy is a function of the number of explorers and their initial distances from p_d.

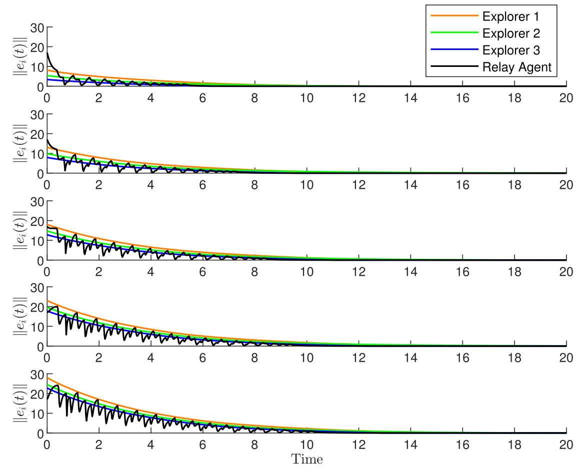

Fig. 17. Normed position tracking errors for 1 relay agent servicing 3 explores. The plots from top to bottom are in correspondence with $R = 5, 10, 15, 20, 25$. For each value of R, the consensus objective was achieved.

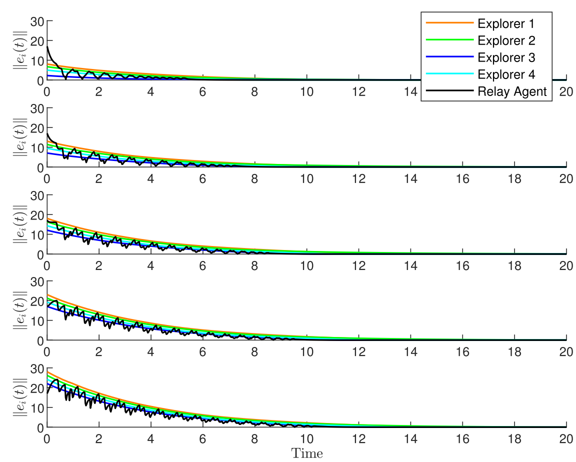

Fig. 18. Normed position tracking errors for 1 relay agent servicing 4 explores. The plots from top to bottom are in correspondence with $R = 5, 10, 15, 20, 25$. For each value of R, the consensus objective was achieved.

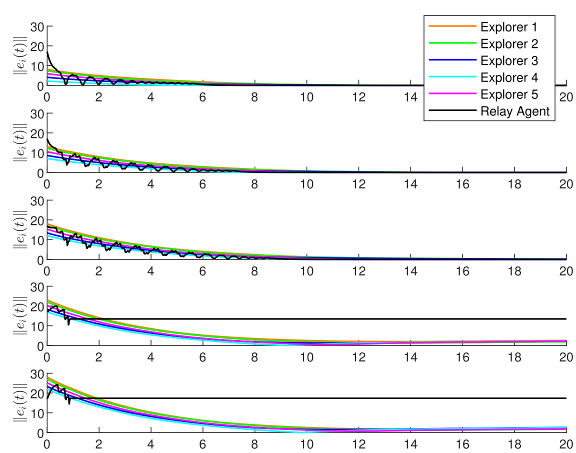

Fig. 19. Normed position tracking errors for 1 relay agent servicing 5 explores. The plots from top to bottom are in correspondence with $R = 5, 10, 15, 20, 25$. The consensus objective was achieved for each value of R except $R \in \{20, 25\}$. Although the explorer positions initially approach p_d since $\|e_i(t)\| \to 0$, these errors slowly diverge as a function of time. Faster rates of divergence occur for larger disturbances.

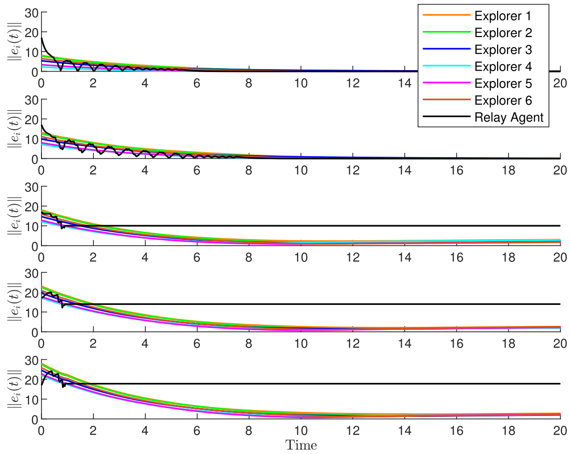

Fig. 20. Normed position tracking errors for 1 relay agent servicing 6 explores. The plots from top to bottom are in correspondence with $R = 5, 10, 15, 20, 25$. The consensus objective was achieved for each value of R except $R \in \{15, 20, 25\}$. Although the explorer positions initially approach p_d since $\|e_i(t)\| \to 0$, these errors slowly diverge as a function of time. Faster rates of divergence occur for larger disturbances.

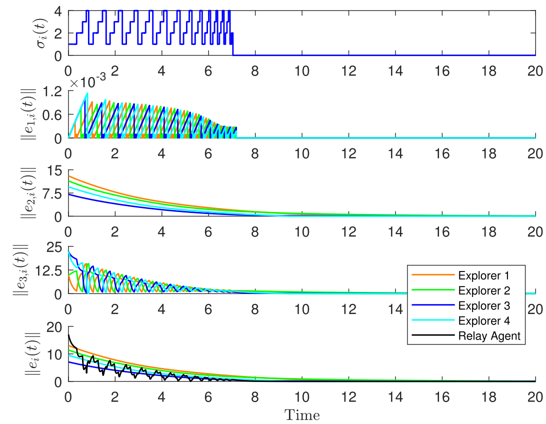

Fig. 21. Simulation results using the exact model knowledge method in [20]. The top plot shows the switching signal that the relay agent uses to service the explorers. Once the explorers are sufficiently close to p_d, the relay agent is regulated to p_d, where this is represented by $\sigma_0(t) = 0$ for $t > 7$. The second plot from the top shows the evolution of $\|e_{1,i}\|$ for each explorer, where $e_{1,i} = \hat{p}_i - p_i$ and $\|e_{1,i}(t)\| < V_T = 1.9$ for all $t \geq 0$ and $i \in F$. Thus, the estimated position trajectory of explorer i is always within a distance of R_{com} from the corresponding true position trajectory. The middle plot shows the evolution of $\|e_{2,i}\|$ for each explorer, which is exponentially driven to 0. Recall that $e_{2,i} = p_d - \hat{p}_i$; hence, the estimated positions of each explorer converge to p_d. The fourth plot from the top shows the $\|e_{3,i}\|$ versus time for each explorer. Each error can be bounded by a nonnegative exponentially decaying function of time since all explorer estimated positions converge to p_d. The bottom plot shows $\|e_i\|$ versus time for each agent, where e_i quantifies the mismatch between the true position of agent i and p_d for $i \in F \cup \{0\}$. The plot shows that the MAS is exponentially regulated to p_d, and, therefore, the consensus objective is achieved.

Fig. 16 shows that the consensus objective is achievable for 1 relay agent servicing 2 explorers with $R \in \{5, 10, 15, 20, 25\}$. The same observation follows for 1 relay agent servicing 3 and 4 explorers as indicated in Figs. 17 and 18. Fig. 19 shows that a MAS with 1 relay agent servicing 5 explorers can accomplish the consensus objective for $R \in \{5, 10, 15\}$. For $R \in \{20, 25\}$, the relay agent is not able to satisfy the maximum dwell-time condition, which, in turn, causes multiple explorers to become lost. Since we do not consider the case where an explorer becomes lost, the relay agent is made to stand still in simulation the moment this occurs, which is represented by a horizontal black line in Fig. 19. When $R \in \{20, 25\}$, the explorers approach p_d; however, they are unable to converge to the desired position. Extending the simulation time results in the divergence of the explorer positions from p_d. Fig. 20 indicates that a MAS with 1 relay agent servicing 6 explorers can achieve the consensus objective for $R \in \{5, 10\}$. When $R \in \{15, 20, 25\}$, the explorers approach p_d; however, they are unable to converge to the desired position. Note that it is possible to realize the objective for larger explorer numbers and values of R under more aggressive controller gains. However, similar trends, i.e., success versus failure in attaining the objective, are observed under such gains. This motivates future work, where the use of communication networks to couple the explorers can be leveraged to facilitate more frequent intermittent state feedback. The coordination of multiple relay agents can also be investigated as a means to increase the rate of feedback.

C. Comparison With Previous Results

In this section, we compare the proposed control strategy with our precursory work in [20] and [21]. In [20], we develop a relay–explorer strategy that enables a MAS to achieve position consensus at a fixed desired location. There are many similarities between [20] and this work, especially in the use of a relay agent to provide intermittent state feedback to each explorer at times determined by a maximum dwell-time condition. However, [20] employed exact model knowledge in the position estimators of the explorers and the maximum dwell-time condition. Since the drift dynamics of each explorer is known, the relay agent does not have to linger with any explorer, i.e., servicing requires the relay agent to provide an explorer with only its current position before leaving to service the next explorer.

In practice, the motion model of an agent may be unknown. Consequently, the result in [20] is not applicable in the absence of exact model knowledge and motivated an adaptive control extension, which we developed in [21]. With respect to [21], the uncertain drift dynamics of an explorer are estimated using a two-layer NN. This NN is then used as a feed-forward model approximation in the position estimator of the corresponding explorer [21, eq. 8]. Note that the work in [21] does not require the relay agent to linger while servicing an explorer. While the work in [21] can attain the consensus objective for a MAS with uncertain explorer drift dynamics, the result does not offer any model learning guarantees. The ability of the relay agent to compute accurate position estimates for each explorer facilitates the consensus objective. In addition, it enables the use of larger dwell-times and the potential to develop extensions that better accommodate scalability.

Simulation results using the methods in [20] and [21] under the same parameter configurations of the baseline case are provided in Figs. 21 and 22, respectively. While lingering by the relay agent is not necessary in neither [20] nor [21], we force the relay agent to linger with each explorer by the same amount of time as in the baseline case. This is done to ensure a direct comparison between all three results. The estimated position dynamics of

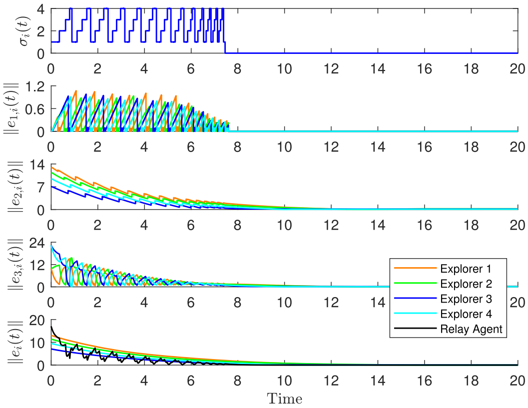

Fig. 22. Simulation results using the two-layer NN method in [21]. The top plot shows the switching signal that the relay agent uses to service the explorers. Once the explorers are sufficiently close to p_d, the relay agent is regulated to p_d, where this is represented by $\sigma_0(t) = 0$ for $t > 7$. The second plot from the top shows the evolution of $\|e_{1,i}\|$ for each explorer, where $e_{1,i} = \hat{p}_i - p_i$ and $\|e_{1,i}(t)\| < V_T = 1.9$ for all $t \geq 0$ and $i \in F$. Thus, the estimated position trajectory of explorer i is always within a distance of R_{com} from the corresponding true position trajectory. The middle plot shows the evolution of $\|e_{2,i}\|$ for each explorer, which is exponentially driven to 0. Recall that $e_{2,i} = p_d - \hat{p}_i$; hence, the estimated positions of each explorer converge to p_d. The fourth plot from the top shows the $\|e_{3,i}\|$ versus time for each explorer. Each error can be bounded by a nonnegative exponentially decaying function of time since all explorer estimated positions converge to p_d. The bottom plot shows $\|e_i\|$ versus time for each agent, where e_i quantifies the mismatch between the true position of agent i and p_d for $i \in F \cup \{0\}$. The plot shows that the MAS is exponentially regulated to p_d, and, therefore, the consensus objective is achieved.

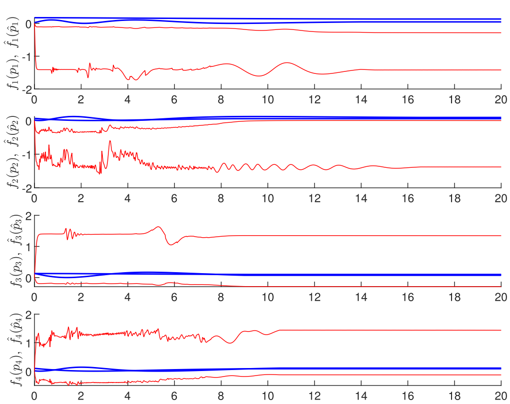

Fig. 23. Each plot shows the componentwise evolution of the true drift dynamics in blue and the corresponding estimated drift dynamics in red for an explorer under the two-layer NN estimation method in [21].

explorer i in [21] take the form $\dot{\hat{p}}_i \triangleq \widehat{W}_i^\top \sigma(\widehat{V}_i^\top \hat{z}_i) + u_i$, where $\widehat{W}_i \in \mathbb{R}^{(L+1)\times m}$, $\widehat{V}_i \in \mathbb{R}^{(m+1)\times L}$, $\hat{z}_i \triangleq [1, \hat{p}_i^\top]^\top \in \mathbb{R}^{m+1}$, and $\sigma : \mathbb{R}^L \to \mathbb{R}^{L+1}$ are the bounded radial basis functions. The left term on the RHS of the $\hat{p}_i$ dynamics reflects the two-layer NN. To ensure as direct of a comparison as possible, we omit the bias term in $\hat{z}_i$, i.e., we redefine the components of the two-layer NN as $\widehat{W}_i \in \mathbb{R}^{L\times m}$, $\widehat{V}_i \in \mathbb{R}^{m\times L}$, $\hat{z}_i \triangleq \hat{p}_i$, and $\sigma : \mathbb{R}^L \to \mathbb{R}^L$. For these simulations, $m = 2$, $L = 3$, and $\sigma(\hat{p}_i) = \phi(\hat{p}_i)$.

In Fig. 21, one can see that the consensus objective is achieved. In addition, $\|e_{1,i}(t)\| \leq 1.2 \times 10^{-3}$ for all $t \geq 0$ and each $i \in F$. Hence, exact model knowledge provides the relay agent with an accurate position estimate of each explorer, where the error in position estimation is due to the random disturbance (with magnitude 10^{-3}). Observe that $V_T = 1.9$ and $\|e_{1,i}(t)\| \leq 1.2 \times 10^{-3}$ for all $t \geq 0$ and each $i \in F$. This implies the Lyapunov stability analysis is conservative, and larger values of V_T can be selected to significantly extend the maximum dwell-time.

In Fig. 22, one can see that the consensus objective is achieved. While $\|e_{1,i}(t)\| < V_T = 1.9$ for all $t \geq 0$ and each $i \in F$, the two-layer NN does not provide as good of a position estimate as the exact model knowledge result. This can be seen by comparing the $\|e_{2,i}\|$ in Figs. 21 and 22. Note that the $\|e_{2,i}\|$ in Fig. 22 exhibits more pronounced jumps than in Fig. 21. This implies that the estimated explorer positions are consistently less accurate under the two-layer NN than under exact model knowledge. With respect to Fig. 14, we can see that $\|e_{1,i}(t)\|$ is substantially smaller during $t \in [4, 7]$ than in Fig. 22. Hence, the RNN with ICL is able to better adapt to model uncertainty than the two-layer NN. Also, the jumps in $\|e_{2,i}\|$ with respect to Fig. 14 are minuscule when compared to those in Fig. 22. In fact, the $\|e_{2,i}\|$ under the RNN with ICL are similar to those generated under exact model knowledge. Comparing the results in Figs. 15 and 23 clearly demonstrates that the RNN with ICL better estimates the explorer drift dynamics than the two-layer NN approach. Hence, a contribution of this work is that the RNN with ICL control strategy is capable of outperforming the two-layer NN result while attaining comparable performance to the exact model knowledge result.

IX. Conclusion

In this article, we investigate the position consensus problem for a relay–explorer MAS. A relay agent switches between multiple explorers based on a maximum dwell-time condition to provide position feedback sufficiently often and enable the explorers to dead reckon to a common, desired location. A Lyapunov-based analysis is used to ensure the stability of individual subsystems, and a switched systems analysis is used to develop maximum dwell-time conditions to ensure overall system stability. Provided the relay agent satisfies the maximum dwell-time conditions, the analysis indicates that position consensus can be achieved despite intermittent state feedback and model uncertainty. Moreover, the proposed strategy enables the relay agent to closely estimate the unknown drift dynamics of each explorer online by leveraging RNNs and ICL, once a finite excitation condition is satisfied. The model estimates can then be communicated to each explorer by the relay agent to enable improved position estimation and facilitate the consensus objective. Experiments validate the performance of the developed control strategy for a MAS of four explorers and a single relay agent, where a physical velocity constraint on the relay agent is considered. Simulations are also conducted to further verify the development, showcase the model estimation benefits afforded by RNNs and ICL in comparison with our previous works, and investigate scalability.

Future efforts will investigate how to coordinate multiple relay agents as well as how to synthesize optimal servicing policies that maximize the number of explores each relay agent can service. Path planning and obstacle avoidance methods are also areas of future investigation. One way to extend the development to include obstacles is to employ a communication network that couples the explorers. Distributed state reconstruction algorithms can then be used by each explorer to estimate the position of every other explorer while simultaneously accounting for course corrections in response to obstacles. These estimates can then be communicated to the relay agent once in range of an explorer, which the relay agent can use to construct a real-time estimate of the physical location of the communication graph, i.e., the location of the nodes as represented by the explorers. The relay agent can then move along the edges of this graph to provide direct feedback to each explorer while ensuring that no explorer is lost.

Acknowledgment

Any opinions, findings, and conclusions or recommendations expressed in this material are those of the author(s) and do not necessarily reflect the views of sponsoring agencies.

Appendix A
Proof of Corollary 8

Proof: Recall that $\rho_i = c_{5,i} + c_{6,i} + k_{1,i} V_T + k_{2,i}\sqrt{m}$ as presented in Theorem 6. Using the equality for ρ_i and $V_T \in (0, R_{\text{com}}/4)$, we see that

$$\frac{2\rho_i}{k_{1,i}} \leq \frac{2\left(c_{5,i} + c_{6,i} + k_{2,i}\sqrt{m}\right)}{k_{1,i}} + \frac{R_{\text{com}}}{2} \tag{67}$$

which can be used to show

$$\frac{4\left(c_{5,i} + c_{6,i} + k_{2,i}\sqrt{m}\right)}{R_{\text{com}}} < k_{1,i} \Longrightarrow \frac{2\rho_i}{k_{1,i}} < R_{\text{com}}.$$

Similarly, we can employ (67) to show

$$\frac{4\left(c_{5,i} + c_{6,i} + k_{2,i}\sqrt{m}\right)}{\sqrt{2}R_{\max} - R_{\text{com}}} < k_{1,i} \Longrightarrow \frac{2\rho_i}{k_{1,i}} < \frac{\sqrt{2}}{2} R_{\max},$$

where $0 < \sqrt{2}R_{\max} - R_{\text{com}}$ provided $\sqrt{2}R_{\text{com}}/2 < R_{\max}$. Hence, $2\rho_i/k_{1,i} < R_{\text{com}}$ and $2\rho_i/k_{1,i} < \sqrt{2}R_{\max}/2$ hold given the sufficient condition in (46). Suppose the relay agent is regulated to p_d once $\|e_i\| \leq 2\rho_i/k_{1,i}$ for all $i \in F$. Then, the relay agent can service all explorers simultaneously, where (4), (7), and (11) imply $e_{2,i} = e_i$. Next, $e_{1,i} = 0_m$, (41), and (42) imply that

$$\begin{aligned}\dot{V}_1\left(\psi_i\right) &\overset{a.e.}{\leq} -e_i^\top N_{6,i} - k_{1,i} e_i^\top e_i - k_{2,i} e_i^\top \operatorname{sgn}\left(e_i\right) \\ &\quad - e_i^\top N_{5,i} \\ &\overset{a.e.}{\leq} -k_{1,i}\left\|e_i\right\|^2 \overset{a.e.}{\leq} -2k_{1,i}\dot{V}_1\left(\psi_i\right)\end{aligned} \tag{68}$$

since $c_{5,i} + c_{6,i} \leq k_{2,i}$. Therefore, (40) and (68) yield $\|e_i(t)\| \leq \|e_i(0)\| e^{-k_{1,i}t}$, where explorer i is exponentially regulated to p_d for each $i \in F$. ■

Appendix B
Proof of Proposition 13

Proof: Substituting (14) into (2) yields $\dot{p}_0 = \widehat{W}_i^\top \phi(\hat{p}_i) + k_3 e_{3,i} + k_4 \operatorname{sgn}(e_{3,i}) + u_i$. Since we aim to compute an upper bound for $k_3(t)$, which applies for all $t \in [t_{n,i}^R, t_{n+1,i}^U]$, (64) implies $\|e_{3,i}\| \leq \|e_{3,i}(t_{n,i}^R)\|$ for all $t \in [t_{n,i}^R, t_{n+1,i}^U]$. Since $u_i \in \mathcal{L}_\infty$ from the proof of Theorem 6, there exists a $u_{i,\max} \in \mathbb{R}_{>0}$ such that $\|u_i(t)\| \leq u_{i,\max}$ for all $t \geq 0$. Using (31), $\|N_{4,i}\| \leq c_{4,i}$, $\|e_{3,i}(t)\| \leq \|e_{3,i}(t_{n,i}^R)\|$, and $\|u_i\| \leq u_{i,\max}$, $\dot{p}_0$ can be upper bounded as $\|\dot{p}_0\| \leq k_3 \|e_{3,i}(t_{n,i}^R)\| + \vartheta_i$. Because $\|\dot{p}_0\| \leq V_{0,\max}$, k_3 must be selected such that $k_3\|e_{3,i}(t_{n,i}^R)\| + \vartheta_i \leq V_{0,\max}$, where (65) follows. ■

Appendix C
Relay–Explorer Algorithm

Algorithm 1: Relay–Explorer Position Consensus Protocol.

Require $t = 0,\ V_T \in (0, R_{\text{com}}/4),\ V_{0,\max} > 0$
Require $\forall_{i\in F}\ \hat{p}_i(0) = p_i(0),\ k_{1,i} > 0,\ k_{2,i} > 0,\ \lambda_i^* > 0$
Require $\forall_{i\in F}\ \widehat{W}_i(0) = 0_{L\times m}$, select basis functions for ϕ
Require $\forall_{i\in F}\ k_{\text{ICL},i} > 0,\ c_{1,i} > 0,\ \Delta t_i^L \in (0, V_T/c_{1,i})$
Require $\forall_{i\in F}\ \Delta t_i \in (0, \Delta t_i^L),\ \rho_i > 0$
Require $\forall_{i\in F}\ \mathcal{YY}_i = 0_{L\times L},\ \mathcal{YX}_i = 0_{L\times m}$
Require $\forall_{i\in F}\ t_i^S = V_T/c_{1,i},\ \vartheta_i \in (0, V_{0,\max})$
Require $k_4 > 0$, select $\sigma_0 \in F$ and $\mathtt{d}t > 0$ (time step)
Require ServiceFlag $=$ True, TimerFlag $=$ True
while $\exists_{i\in F}\ \|p_i - p_d\| > 0$ **do**
  if ServiceFlag **then**
    $t_{\sigma_0}^R \leftarrow t,$
    $e_{3,\sigma_0} \leftarrow \hat{p}_{\sigma_0} - p_0$
    $k_{3,\max} \leftarrow (V_{0,\max} - \vartheta_i)/\|e_{3,\sigma_0}\|$
    $k_3 \leftarrow \ln(\|e_{3,\sigma_0}\|/(R_{\text{com}} - V_T))/(t_{\sigma_0}^S - t_{\sigma_0}^R)$
    if $k_3 > k_{3,\max}$ **then**
      $k_3 \leftarrow k_{3,\max}$
    end if
    ServiceFlag $\leftarrow$ False
  end if
  for $i \in F$
    $e_{2,i} \leftarrow p_d - \hat{p}_i$
    $u_i \leftarrow k_{1,i} e_{2,i} + k_{2,i}\operatorname{sgn}(e_{2,i})$
    $\dot{p}_i \leftarrow f_i(p_i) + u_i + d_i$
    $\dot{\hat{p}}_i \leftarrow \widehat{W}_i^\top \phi(\hat{p}_i) + u_i$
    if $\lambda_{\min}(\mathcal{YY}_i) > \lambda_i^*$ **then**
      $G_i \leftarrow k_{\text{ICL},i}(\mathcal{YX}_i - \mathcal{YY}_i \widehat{W}_i)$
      $\mu_i \leftarrow \operatorname{vec}(G_i)$
      $\omega_i \leftarrow \operatorname{vec}(\widehat{W}_i)$
      $\dot{\omega}_i \leftarrow \operatorname{proj}(\mu_i, \omega_i)$
    else
      $\dot{\omega}_i \leftarrow 0_{Lm}$
    end if
  end for
  $e_{3,\sigma_0} \leftarrow \hat{p}_{\sigma_0} - p_0$
  $e_{2,\sigma_0} \leftarrow p_d - \hat{p}_{\sigma_0}$
  $u_{\sigma_0} \leftarrow k_{1,\sigma_0} e_{2,\sigma_0} + k_{2,\sigma_0}\operatorname{sgn}(e_{2,\sigma_0})$
  $\bar{u}_0 \leftarrow k_3 e_{3,\sigma_0} + k_4 \operatorname{sgn}(e_{3,\sigma_0})$
  $u_0 \leftarrow \widehat{W}_{\sigma_0}^\top \phi(\hat{p}_{\sigma_0}) + u_{\sigma_0} + \bar{u}_0$

Algorithm 2: Relay-Explorer Position Consensus Protocol *(Continued)*.

if $\|p_0 - p_{\sigma_0}\| \leq R_{\text{com}}$ **then**
  $\hat{p}_{\sigma_0} \leftarrow p_{\sigma_0},\ t^S_{\sigma_0} \leftarrow t + V_T/c_{1,i}$
  if TimerFlag **then**
    timer $\leftarrow 0$
    $y_{\sigma_0} \leftarrow 0_L$
    $x_{\sigma_0} \leftarrow -p_{\sigma_0}$
    TimerFlag $\leftarrow$ False
  end if
  if timer $< \Delta t_{\sigma_0}$ **then**
    $y_{\sigma_0} \leftarrow y_{\sigma_0} + \phi(p_{\sigma_0}) \cdot \mathtt{d}t$
    $x_{\sigma_0} \leftarrow x_{\sigma_0} - u_{\sigma_0} \cdot \mathtt{d}t$
    $\mathcal{YX}_{\sigma_0} \leftarrow \mathcal{YX}_{\sigma_0} + y_{\sigma_0} x_{\sigma_0}^\top$
    $\mathcal{YY}_{\sigma_0} \leftarrow \mathcal{YY}_{\sigma_0} + y_{\sigma_0} y_{\sigma_0}^\top$
  else if timer $= \Delta t_{\sigma_0}$ **then**
    $y_{\sigma_0} \leftarrow y_{\sigma_0} + \phi(p_{\sigma_0}) \cdot \mathtt{d}t$
    $x_{\sigma_0} \leftarrow x_{\sigma_0} + p_{\sigma_0} - u_{\sigma_0} \cdot \mathtt{d}t$
    $\mathcal{YX}_{\sigma_0} \leftarrow \mathcal{YX}_{\sigma_0} + y_{\sigma_0} x_{\sigma_0}^\top$
    $\mathcal{YY}_{\sigma_0} \leftarrow \mathcal{YY}_{\sigma_0} + y_{\sigma_0} y_{\sigma_0}^\top$
  end if
  if timer $\geq \Delta t^L_{\sigma_0}$ **then**
    TimerFlag $\leftarrow$ True, ServiceFlag $\leftarrow$ True
    $\sigma_0 \leftarrow \sigma_0 + 1$
    if $\sigma_0 > N$ **then**
      $\sigma_0 \leftarrow 1$
    end if
  end if
end if
for $i \in F$ **do**
  $e_i \leftarrow p_d - p_i$
end for
if $\forall_{i \in F}\ \|e_i\| \leq 2\rho_i / k_{1,i}$ **then**
  $u_0 \leftarrow k_3(p_d - p_0)$
end if
$\dot{p}_0 \leftarrow u_0$
for $i \in F$ **do**
  $p_i \leftarrow p_i + \dot{p}_i \cdot \mathtt{d}t,\ \hat{p}_i \leftarrow \hat{p}_i + \dot{\hat{p}}_i \cdot \mathtt{d}t$
  $\omega_i \leftarrow \omega_i + \dot{\omega}_i \cdot \mathtt{d}t,\ \widehat{W}_i \leftarrow \mathrm{vec}^{-1}(\omega_i)$
end for
$p_0 \leftarrow p_0 + \dot{p}_0 \cdot \mathtt{d}t$
timer $\leftarrow$ timer $+ \mathtt{d}t$
$t \leftarrow t + \mathtt{d}t$
end while

REFERENCES

[1] R. Khodayi-Mehr, Y. Kantaros, and M. M. Zavlanos, "Distributed state estimation using intermittently connected robot networks," *IEEE Trans. Robot.*, vol. 35, no. 3, pp. 709–724, Jun. 2019.

[2] P. B. g. Dohmann and S. Hirche, "Distributed control for cooperative manipulation with event-triggered communication," *IEEE Trans. Robot.*, vol. 36, no. 4, pp. 1038–1052, Aug. 2020.

[3] Y. Liu et al., "A distributed control approach to formation balancing and maneuvering of multiple multirotor uavs," *IEEE Trans. Robot.*, vol. 34, no. 4, pp. 870–882, Aug. 2018.

[4] A. Trotta, M. D. Felice, F. Montori, K. R. Chowdhury, and L. Bononi, "Joint coverage, connectivity, and charging strategies for distributed uav networks," *IEEE Trans. Robot.*, vol. 34, no. 4, pp. 883–900, Aug. 2018.

[5] R. Olfati-Saber, J. A. Fax, and R. M. Murray, "Consensus and cooperation in networked multi-agent systems," *Proc. IEEE*, vol. 95, no. 1, pp. 215–233, Jan. 2007.

[6] W. Ren and R. W. Beard, *Distributed Consensus in Multi-Vehicle Cooperative Control*. New York, NY,USA: Springer, 2008.

[7] Q. Hui and W. M. Haddad, "Distributed nonlinear control algorithms for network consensus," *Automatica*, vol. 44, no. 9, pp. 2375–2381, 2008.

[8] X. Wang and M. Lemmon, "Self-triggered feedback control systems with finite-gain $\mathcal{L}_2$ stability," *IEEE Trans. Autom. Control*, vol. 54, no. 3, pp. 452–467, Mar. 2009.

[9] W. Heemels and M. Donkers, "Model-based periodic event-triggered control for linear systems," *Automatica*, vol. 49, no. 3, pp. 698–711, 2013.

[10] X. Meng and T. Chen, "Event based agreement protocols for multi-agent networks," *Automatica*, vol. 49, pp. 2125–2132, Jul. 2013.

[11] J. M. Esposito, "Maintaining wireless connectivity constraints for robot swarms in the presence of obstacles," *J. Robot.*, vol. 2011, no. 571485, 2011.

[12] H. Li, X. Liao, T. Huang, and W. Zhu, "Event-triggering sampling based leader-following consensus in second-order multi-agent systems," *IEEE Trans. Autom. Control*, vol. 60, no. 7, pp. 1998–2003, Jul. 2015.

[13] T. H. Cheng, Z. Kan, J. R. Klotz, J. M. Shea, and W. E. Dixon, "Event-triggered control of multi-agent systems for fixed and time-varying network topologies," *IEEE Trans. Autom. Control*, vol. 62, no. 10, pp. 5365–5371, Oct. 2017.

[14] F. Zegers, P. Deptula, J. M. Shea, and W. E. Dixon, "Event/self-triggered approximate leader-follower consensus with resilience to byzantine adversaries," *IEEE Trans. Autom. Control*, vol. 67, no. 3, pp. 1356–1370, Mar. 2022.

[15] F. Zegers, M. Hale, J. M. Shea, and W. E. Dixon, "Event-triggered formation control and leader tracking with resilience to byzantine adversaries: A reputation-based approach," *IEEE Trans. Control Netw. Syst.*, vol. 8, no. 3, pp. 1417–1429, Sep. 2021.

[16] C. Nowzari and G. J. Pappas, "Multi-agent coordination with asynchronous cloud access," in *Proc. IEEE Amer. Control Conf.*, 2016, pp. 4649–4654.

[17] A. Adaldo, D. Liuzza, D. V. Dimarogonas, and K. H. Johansson, "Cloud-supported formation control of second-order multi-agent systems," *IEEE Trans. Control Netw. Syst.*, vol. 5, no. 4, pp. 1563–1574, Dec. 2018.

[18] S. L. Bowman, C. Nowzari, and G. J. Pappas, "Consensus of multiagent systems via asynchronous cloud communication," *IEEE Trans. Control Netw. Syst.*, vol. 7, no. 2, pp. 627–637, Jun. 2020.

[19] H.-Y. Chen, Z. I. Bell, P. Deptula, and W. E. Dixon, "A switched systems framework for path following with intermittent state feedback," *IEEE Control Syst. Lett.*, vol. 2, no. 4, pp. 749–754, Oct. 2018.

[20] F. Zegers, H.-Y. Chen, P. Deptula, and W. E. Dixon, "Distributed coordination of a multi-agent system with intermittent communication: A switched systems approach," in *Proc. ASME Dyn. Syst. Control Conf*, 2018, pp. 2372–2377.

[21] F. Zegers, H.-Y. Chen, P. Deptula, and W. E. Dixon, "A switched systems approach to consensus of a distributed multi-agent system with intermittent communication," in *Proc. IEEE Amer. Control Conf.*, 2019, pp. 2372–2377.

[22] A. Parikh, R. Kamalapurkar, and W. E. Dixon, "Integral concurrent learning: Adaptive control with parameter convergence using finite excitation," *Int J. Adapt. Control Signal Process*, vol. 33, no. 12, pp. 1775–1787, Dec. 2019.

[23] W. Rudin, *Principles of Mathematical Analysis*. New York, NY, USA: McGraw-Hill, 1976.

[24] F. L. Lewis, R. Selmic, and J. Campos, *Neuro-Fuzzy Control of Industrial Systems With Actuator Nonlinearities*. Philadelphia, PA, USA: Soc. Ind. Appl. Math., 2002.

[25] Z. Bell, P. Deptula, H.-Y. Chen, E. Doucette, and W. E. Dixon, "Velocity and path reconstruction of a moving object using a moving camera," in *Proc. IEEE Amer. Control Conf.*, 2018, pp. 5256–5261.

[26] Z. Cai, M. S. de Queiroz, and D. M. Dawson, "A sufficiently smooth projection operator," *IEEE Trans. Autom. Control*, vol. 51, no. 1, pp. 135–139, Jan. 2006.

[27] Y. Kikuya, S. M. Dibaji, and H. Ishii, "Fault-tolerant clock synchronization over unreliable channels in wireless sensor networks," *IEEE Trans. Control Netw. Syst.*, vol. 5, no. 4, pp. 1551–1562, 2018.

[28] M. Guarro and R. G. Sanfelice, "Hyntp: An adaptive hybrid network time protocol for clock synchronization in heterogeneous distributed systems," in *Proc. IEEE Amer. Control Conf.*, 2020, pp. 1025–1030.

[29] B. E. Paden and S. S. Sastry, "A calculus for computing Filippov's differential inclusion with application to the variable structure control of robot manipulators," *IEEE Trans. Circuits Syst.*, vol. 34, no. 1, pp. 73–82, Jan. 1987.

[30] D. Shevitz and B. Paden, "Lyapunov stability theory of nonsmooth systems," *IEEE Trans. Autom. Control*, vol. 39, no. 9, pp. 1910–1914, Sep. 1994.

[31] Z. Xu, F. M. Zegers, B. Wu, W. E. Dixon, and U. Topcu, "Controller synthesis for multi-agent systems with intermittent communication: A metric temporal logic approach," in *Proc. IEEE Allerton Conf. Commun., Control, Comput*., 2019, pp. 1015–1022.

[32] D. Le, X. Luo, L. Bridgeman, M. Zavlanos, and W. E. Dixon, "Single-agent indirect herding of multiple targets using metric temporal logic switching," in *Proc. IEEE Conf. Decis. Control*, 2020, pp. 1398–1403.

[33] F. M. Zegers, P. Deptula, H.-Y. Chen, A. Isaly, and W. E. Dixon, "Experiment for a switched systems approach to multi-agent consensus: A relay-explorer perspective," Accessed: May. 11, 2021. [Online]. Available: https://youtu.be/HyxTTsRqGwY

[34] R. Sanfelice, D. Copp, and P. Nanez, "A Toolbox for Simulation of Hybrid Systems in matlab/simulink: Hybrid Equations (hyeq) Toolbox," in *Proc. Int. Conf. Hybrid Syst., Comp. Control*, 2013, pp. 101–106.

Federico M. Zegers (Member, IEEE) received the Ph.D. degree in mechanical engineering from the Department of Mechanical and Aerospace Engineering, University of Florida, Gainesville, FL, USA, in 2021.

In June 2017, Federico joined the Nonlinear Controls and Robotics group as a Ph.D. Student working under the guidance of Dr. Warren Dixon. He is currently a Research Aerospace Engineer with Air Force Research Laboratory, Eglin Air Force Base, Eglin, FL, USA. His research interests include robotics, Lyapunov-based nonlinear and adaptive control, switched and hybrid systems, and multiagent systems.

Dr. Zegers was the recipient of the 2020 Graduate Student Research Award in Dynamics, Systems, and Control.

Patryk Deptula received the B.Sc. (with High Hons.) degree in mechanical engineering (major) and mathematics (minor) from Central Connecticut State University, New Britain, CT, USA, in 2014, and the M.S. and Ph.D. degrees in mechanical engineering from the Department of Mechanical and Aerospace Engineering, University of Florida, Gainesville, FL, USA, in 2017 and 2019, respectively.

He performed research related to hybrid propellant rocket engines as an undergraduate. During his graduate studies, his research was on nonlinear controls and autonomy, with a focus on learning-based and adaptive control in a variety of applications. His current research interests include, but are not limited to, multiagent systems, human–machine interaction, vision-based navigation and control, and robotics applied to a variety of fields.

Hsi-Yuan Chen received the Ph.D. degree in mechanical engineering from the University of Florida, Gainesville, FL, USA, in 2018.

In 2019, he joined Amazon Robotics, North Reading, MA, USA, where he is currently an Applied Scientist with a focus on autonomous mobility. His research interests include the development and application of Lyapunov-based state estimation, and control methods for autonomous vehicles.

Axton Isaly received the B.S. degree in mechanical engineering in 2019 from the University of Florida, Gainesville, FL, USA, where he is currently working toward the Ph.D. degree in mechanical engineering under the supervision of Dr. Warren Dixon.

His research interests include safe control synthesis via control barrier functions and hybrid system theory.

Warren E. Dixon (Fellow, IEEE) received the Ph.D. degree in electrical engineering from the Department of Electrical and Computer Engineering, Clemson University, Clemson, SC, USA, in 2000.

He was a Research Staff Member and Eugene P. Wigner Fellow with Oak Ridge National Laboratory (ORNL), Oak Ridge, TN, USA, until 2004, and then, he joined the Mechanical and Aerospace Engineering Department, University of Florida, Gainesville, FL, USA, where he is currently the Dean's Leadership Professor and Department Chair. His research interests include the development and application of Lyapunov-based control techniques for uncertain nonlinear systems.

Dr. Dixon was the recipient of the 2015 and 2009 American Automatic Control Council (AACC) O. Hugo Schuck (Best Paper) Award, 2013 Fred Ellersick Award for Best Overall MILCOM Paper, 2011 American Society of Mechanical Engineers (ASME) Dynamics Systems and Control Division Outstanding Young Investigator Award, Air Force Commander's Public Service Award (2016) for his contributions to the U.S. Air Force Science Advisory Board, and 2006 IEEE Robotics and Automation Society (RAS) Early Academic Career Award. He is an ASME Fellow. He is currently or formerly an Associate Editor for *ASME Journal of Dynamic Systems, Measurement and Control, Automatica*, IEEE Control Systems, IEEE Transactions on Systems Man and Cybernetics: Part B Cybernetics, and *International Journal of Robust and Nonlinear Control*.